# Coupler Position Optimization and Channel Estimation for Flexible Coupler Antenna Aided Multiuser Communication

Xiaodan Shao, *Member, IEEE*, Chuangye Shan, Weihua Zhuang, *Fellow, IEEE*, and Xuemin Shen, *Fellow, IEEE*

***Abstract*—In this paper, we propose a flexible coupler antenna (FCA), also referred to as a reconfigurable coupler antenna (RCA), to enhance wireless communication performance at low hardware cost. At each FCA, there is one fixed-position active antenna and multiple passive couplers that can move within a designated region around the active antenna. Moreover, each FCA is equipped with a local processing unit (LPU). All LPUs exchange signals with a central processing unit (CPU) for joint signal processing. We study an FCA-aided multiuser multiple-input multiple-output (MIMO) system, where an FCA array base station (BS) is deployed to enhance the downlink communication between the BS and multiple single-antenna users. We formulate optimization problems to maximize the achievable sum rate of users by jointly optimizing the coupler positions and digital beamforming, subject to movement constraints on the coupler positions and the transmit power constraint. To address the resulting nonconvex optimization problem, the digital beamforming is expressed as a function of the coupler position vectors, which are then optimized using the proposed distributed coupler position optimization algorithm. Considering a structured time domain pattern of pilots and coupler positions, pilot-assisted centralized and distributed channel estimation algorithms are designed under the FCA array architecture. Simulation results demonstrate that the distributed FCA array achieves substantial rate gains over conventional benchmarks in multiuser systems without moving active antennas, and approaches the performance of fully active arrays while significantly reducing hardware cost. Moreover, the proposed centralized channel estimation outperforms the benchmark schemes in terms of both pilot overhead and channel reconstruction accuracy, while the distributed scheme provides a favorable accuracy and complexity tradeoff by shifting computations to the LPUs.**

***Index Terms*—Flexible coupler antenna (FCA), coupler position optimization, distributed optimization, channel estimation, mechanical beamforming, mutual coupling.**

## I. Introduction

MULTIPLE-INPUT multiple-output (MIMO) is an important enabling technique for sixth-generation (6G) and beyond systems, since it can serve multiple mobile users on the same resource block concurrently [1], [2], [3], [4]. For instance, extremely large-scale MIMO can achieve significantly higher achievable rates by using more antennas than existing massive MIMO within a given space [5]. Passive MIMO, also known as intelligent reflecting surfaces (IRS)/reconfigurable intelligent surfaces (RIS), can enhance wireless network capacity in a cost-effective manner [6], [7], [8], [9], [10]. An appealing property of MIMO is that its performance gains scale with the number of antennas. Traditional MIMO systems, however, face two main challenges. First, higher data rates often require more antennas and thus larger installation space. Moreover, conventional MIMO typically requires a dedicated radio-frequency (RF) chain for each antenna, which increases hardware cost, power consumption, and transceiver size, and makes MIMO systems costly and bulky. Second, antennas in conventional MIMO systems are deployed at fixed positions, which limits the ability to adaptively reconfigure or optimize the wireless channel according to user distribution and environmental variations.

On the other hand, most existing works on MIMO systems assume a centralized processing architecture, where a central processing unit (CPU) is connected to all antennas [1]. In such systems, the received signals must be collected at the CPU to execute key tasks such as signal precoding and detection as well as channel estimation. As the number of antennas increases, centralized processing leads to significantly higher computational cost and complexity, together with longer processing delay, which may hinder the practical deployment of large-scale antenna arrays in future wireless networks. Moreover, centralized algorithms typically incur large communication cost between the antennas and the baseband processor, and they also require high computational cost due to large-scale signal processing [11], [12], [13], [14]. These issues call for a powerful and expensive CPU, which may become impractical or unaffordable when the antenna array size is large.

To overcome the above limitations, we propose in this paper a new distributed flexible coupler antenna (FCA) array, as illustrated in Fig. 1, where each FCA is equipped with a local processing unit (LPU) to enable decentralized and parallel processing, thereby alleviating the computational burden at the CPU while improving communication performance. Moreover, by dispensing with the requirement that each antenna be connected to a dedicated RF chain, the FCA array consists of multiple

Received 8 February 2026; revised 9 April 2026; accepted 14 May 2026. Date of publication 19 May 2026; date of current version 21 September 2026. This work was supported by the Natural Sciences and Engineering Research Council (NSERC) of Canada. The review of this article was coordinated by Prof. Hai Lin. *(Corresponding author: Chuangye Shan.)*

Xiaodan Shao, Weihua Zhuang, and Xuemin Shen are with the Department of Electrical and Computer Engineering, University of Waterloo, Waterloo, ON N2L 3G1, Canada (e-mail: x6shao@uwaterloo.ca; wzhuang@uwaterloo.ca; sshen@uwaterloo.ca).

Chuangye Shan is with the Shell (Beijing) New Energy Technology Company, Ltd., Beijing 100027, China (e-mail: chuangyeshan@outlook.com).

Digital Object Identifier 10.1109/TVT.2026.3694777

0018-9545 © 2026 IEEE. All rights reserved, including rights for text and data mining, and training of artificial intelligence and similar technologies. Personal use is permitted, but republication/redistribution requires IEEE permission. See https://www.ieee.org/publications/rights/index.html for more information.

Authorized licensed use limited to: Nanjing University. Downloaded on October 30,2026 at 06:12:46 UTC from IEEE Xplore. Restrictions apply.

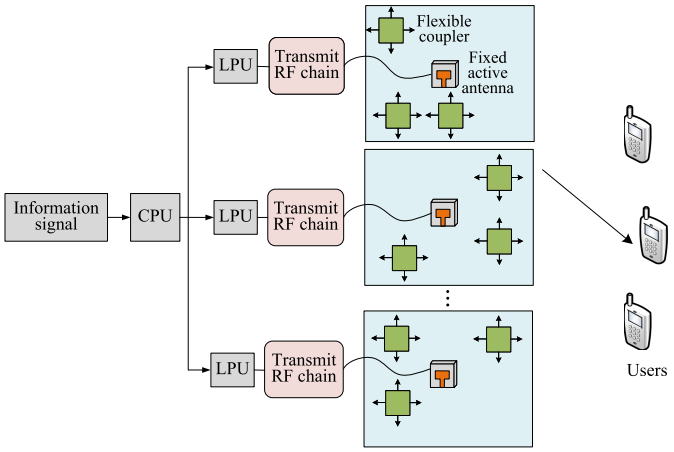



Fig. 1. Proposed distributed FCA array for multiuser systems.

FCAs, each comprising a single active antenna connected to one RF chain and multiple passive couplers. The passive couplers are not directly fed and do not require dedicated RF chains. They can be independently adjusted in position around their associated active antenna, while the active antenna remains fixed at the transceiver. By exploiting coupler movement and the mutual coupling between neighboring antenna and coupler elements, the passive couplers radiate through excitation induced by their associated active antenna. In the proposed distributed FCA array, all LPUs operate in a decentralized and parallel manner and exchange signals with the CPU for joint signal processing, such as channel estimation, precoding, and combining. The proposed architecture leverages both the CPU and the LPUs to not only offload computational tasks from the CPU but also alleviate the fronthaul communication burden between the distributed FCAs and the CPU by exploiting local computation and baseband signal processing at the LPUs. This advantage becomes more pronounced in large-scale deployments where fronthaul bandwidth is limited or where a single central baseband processor becomes a bottleneck. As a result, the proposed architecture can reduce the overall processing burden and communication overhead at the system level. Detailed hardware-level evaluation is left for future work.

Different from six-dimensional movable antennas (6DMA) [15], [16], [17], [18], [19], [20], which enhance communication performance by translating and/or rotating active antennas together with their RF chains over relatively large regions, in a distributed FCA system, only the passive couplers are repositioned within a small local region where electromagnetic coupling is strong, while the active antennas and their RF chains remain fixed. This design substantially reduces transmit power consumption and mechanical control complexity, and enables faster and more practical position reconfiguration. Thus, the distributed FCA array features advantages such as a compact structure, low profile, and lightweight, which make it suitable for small-sized terminals and practical deployment. This complexity-performance tradeoff is most attractive in slowly time-varying channel conditions, or when the coupler positions are updated on a slower timescale based on statistical channel state information (CSI).

The main contributions of this paper are summarized as follows.

- We propose a distributed FCA array to enhance communication performance and reduce centralized processing complexity by equipping each FCA with a local LPU. The FCA array consists of multiple FCAs, each containing one fixed-position active antenna and multiple passive couplers that can move within a designated region around each active antenna to enhance the multiuser communication. The distributed FCA array features a compact structure without moving the active antennas and their RF chains, making it particularly attractive for large-scale antenna deployments in small-sized devices.
- Based on the distributed FCA array, we formulate an optimization problem to maximize the achievable sum rate of users by determining the positions of the passive couplers and the transmit beamforming, subject to their practical movement and transmit power constraints. To solve this nonconvex problem, we develop a successive convex approximation (SCA)-based distributed coupler-position optimization algorithm, where the LPUs update the coupler positions in parallel via local projections and the CPU broadcasts the required gradient information and updates the minimum mean square error (MMSE) precoder.
- By exploiting a structured training protocol with multiple pilot blocks and blockwise fixed coupler positions, we develop two pilot-assisted channel estimation algorithms under the distributed FCA architecture, namely, centralized scheme and distributed scheme. In the centralized scheme, the CPU stacks pilot-correlated observations across all FCAs and performs sparse recovery to estimate the angular support and path gains, enabling channel reconstruction for arbitrary coupler positions. In the distributed scheme, each LPU conveys low-overhead support information to the CPU, which carries out lightweight fusion and path gain estimation using low-dimensional statistics.
- Extensive simulations validate the effectiveness of the proposed FCA array and the associated optimization and channel estimation designs. The results show that the proposed FCA array can closely approach the achievable rate of a fully active array while using significantly fewer active antennas, due to the interference mitigation, mechanical beamforming gain, and fading mitigation enabled by coupler repositioning. Moreover, simulations demonstrate the efficiency of the proposed channel estimation schemes.

The remainder of this paper is organized as follows. Section II describes the system model. Section III formulates the optimization problem for maximizing the achievable sum rate through coupler position design and then presents the proposed distributed coupler position optimization algorithm. Section IV presents the proposed centralized and distributed channel estimation algorithms for the designed FCA array. Section V provides numerical results and corresponding discussions. Finally, Section VI concludes this work.

*Notations:* Boldface uppercase and lowercase letters denote matrices and vectors, respectively, $(\cdot)^*$, $(\cdot)^H$, and $(\cdot)^T$ denote complex conjugation, conjugate transpose, and transpose,

Authorized licensed use limited to: Nanjing University. Downloaded on October 30,2026 at 06:12:46 UTC from IEEE Xplore. Restrictions apply.

respectively. For scalar $a$, $|a|$ denotes its magnitude. For vector $\mathbf{a}$, $\|\mathbf{a}\|_2$ denotes the $\ell_2$ norm. For matrix $\mathbf{A}$, $\|\mathbf{A}\|_F$ denotes the Frobenius norm. Operator $\mathrm{diag}(\mathbf{x})$ denotes a diagonal matrix whose diagonal is $\mathbf{x}$, $[\mathbf{a}]_j$ denotes the $j$-th entry of vector $\mathbf{a}$, $\mathbb{E}[\cdot]$ denotes statistical expectation, $[\mathbf{A}]_{i,j}$ denotes the $(i,j)$-th entry of a matrix $\mathbf{A}$, $[\mathbf{A}]_{:,k}$ and $[\mathbf{A}]_{k,:}$ denote the $k$-th column and the $k$-th row of $\mathbf{A}$, respectively, $\mathbf{I}_M$ denotes the $M \times M$ identity matrix, $\mathrm{blkdiag}\{\mathbf{A}_1, \ldots, \mathbf{A}_M\}$ denotes a block-diagonal matrix with diagonal sub-matrices given by $\mathbf{A}_1, \ldots, \mathbf{A}_M$, $\mathbb{R}$ and $\mathbb{C}$ denote the real and complex fields, respectively, $\mathcal{CN}(0, \sigma^2)$ denotes a complex Gaussian distribution with mean 0 and variance $\sigma^2$, $\Re\{\cdot\}$ denotes the real part of a complex quantity, $|\mathcal{I}|_{\mathrm{c}}$ denotes the cardinality of index set $\mathcal{I}$, $\mathrm{supp}(\mathbf{x})$ denotes the support set of vector $\mathbf{x}$, $\mathrm{tr}(\cdot)$ denotes the trace of a square matrix, and $\nabla f(\mathbf{x})$ denotes the gradient of function $f$ with respect to $\mathbf{x}$.

## II. System Model

### A. Distributed Flexible Coupler Array

As shown in Fig. 1, the proposed FCA array consists of $M$ FCAs. Each FCA comprises one fixed-position active antenna and $N$ passive couplers, which can move within a designated region, i.e., $\mathcal{C}_m$ surrounding the $m$-th active antenna. Each active antenna is connected to a single RF chain and serves as the directly excited radiation source in each FCA. In contrast, the passive couplers are not directly fed and do not require additional RF chains. Instead, they radiate through induced currents excited by their associated active antenna via near-field electromagnetic coupling. The positions of passive couplers are mechanically adjustable with the aid of actuation components such as micro-electro-mechanical systems (MEMS), which offer low power consumption and fast response. Moreover, each FCA is equipped with local computing hardware, i.e., an LPU, which carries out the necessary baseband processing tasks, such as channel estimation and signal precoding and combining, in a decentralized and parallel fashion, as shown in Fig. 1. Each LPU is connected to the common CPU at the base station (BS) via separate flexible cables, such as coaxial cables. These cables supply power to the FCA and also facilitate control and signal exchange between the LPU and the CPU. The users are each assumed to be equipped with a single fixed-position antenna. By reconfiguring only the passive coupler positions within a small local region, the proposed FCA array enhances wireless communication performance while avoiding the movement of active antennas or RF chains, thereby significantly reducing mechanical control complexity and energy consumption.

### B. Channel Model

As illustrated in Fig. 1, we consider a downlink multiuser wireless communication system where an FCA array is deployed at the BS. The BS serves $K$ single-antenna users. The FCA array can be reconfigured by mechanically adjusting the positions of its passive couplers.

We adopt a two-dimensional Cartesian coordinate system. The transmit array lies in the $x$–$y$ plane. The $M$ active antennas form a uniform linear array along the $y$-axis. The first active antenna is located at origin $\mathbf{q}_1 = [0, 0]^{\mathrm{T}}$ and the $m$-th active antenna is located at

$$\mathbf{q}_m = [0, (m-1)d_y]^{\mathrm{T}}, \quad m \in \mathcal{M}, \tag{1}$$

where $\mathcal{M} = \{1, 2, \ldots, M\}$ and $d_y$ denotes the spacing between adjacent active antennas.

Let $\mathcal{K} = \{1, 2, \ldots, K\}$ denote the set of user indices. For user $k \in \mathcal{K}$, we consider a narrowband geometric multipath channel with $L_k$ paths. The azimuth angle of departure of the $\ell$-th path from the BS is denoted by $\phi_{k,\ell}$ and the corresponding complex path gain is denoted by $\alpha_{k,\ell}$, $\ell = 1, 2, \ldots, L_k$. Let $\lambda$ denote the carrier wavelength. The steering vector of the active-antenna array for angle $\phi_{k,\ell}$ is given by

$$\mathbf{a}_y(\phi_{k,\ell}) = \left[1,\, e^{-j\frac{2\pi}{\lambda} d_y \sin\phi_{k,\ell}},\, \ldots,\, e^{-j\frac{2\pi}{\lambda}(M-1)d_y \sin\phi_{k,\ell}}\right]^{\mathrm{T}}. \tag{2}$$

The channel vector between all active antennas and user $k$ is

$$\mathbf{h}_{\mathrm{A},k} = \sum_{\ell=1}^{L_k} \alpha_{k,\ell}\, \mathbf{a}_y(\phi_{k,\ell}) \in \mathbb{C}^{M\times 1}. \tag{3}$$

The two-dimensional position of the $n$-th coupler associated with the $m$-th active antenna is

$$\mathbf{p}_{n,m} = [x_{n,m},\, y_{n,m}]^{\mathrm{T}} \in \mathbb{R}^2, \quad n \in \mathcal{N},\ m \in \mathcal{M}, \tag{4}$$

where $\mathcal{N} = \{1, 2, \ldots, N\}$. We collect all coupler positions into vector

$$\mathbf{p} = \left[\mathbf{p}_1^{\mathrm{T}}, \mathbf{p}_2^{\mathrm{T}}, \ldots, \mathbf{p}_M^{\mathrm{T}}\right]^{\mathrm{T}}, \tag{5}$$

where $\mathbf{p}_m = [\mathbf{p}_{1,m}^{\mathrm{T}}, \mathbf{p}_{2,m}^{\mathrm{T}}, \ldots, \mathbf{p}_{N,m}^{\mathrm{T}}]^{\mathrm{T}} \in \mathbb{R}^{2N}$ is the position vector of the couplers in the $m$-th FCA.

For user $k$ and its $\ell$-th path, we denote the two-dimensional direction vector in the $x$–$y$ plane as

$$\boldsymbol{\kappa}_{k,\ell} = [\cos\phi_{k,\ell},\, \sin\phi_{k,\ell}]^{\mathrm{T}} \in \mathbb{R}^2. \tag{6}$$

The coupler steering vector for user $k$ on path $\ell$ is given by

$$\mathbf{a}_{\mathrm{C},k,\ell}(\mathbf{p}) = \left[\mathbf{a}_{\mathrm{C},k,\ell}(\mathbf{p}_1)^{\mathsf{T}}, \mathbf{a}_{\mathrm{C},k,\ell}(\mathbf{p}_2)^{\mathsf{T}}, \ldots, \mathbf{a}_{\mathrm{C},k,\ell}(\mathbf{p}_M)^{\mathsf{T}}\right]^{\mathsf{T}}, \tag{7}$$

where $\mathbf{a}_{\mathrm{C},k,\ell}(\mathbf{p}_m)$ denotes the coupler steering vector associated with user $k$, path $\ell$, and the $m$-th FCA, and is given by

$$\mathbf{a}_{\mathrm{C},k,\ell}(\mathbf{p}_m) = \left[e^{-j\frac{2\pi}{\lambda}\boldsymbol{\kappa}_{k,\ell}^{\mathsf{T}}\mathbf{p}_{1,m}}, \ldots, e^{-j\frac{2\pi}{\lambda}\boldsymbol{\kappa}_{k,\ell}^{\mathsf{T}}\mathbf{p}_{N,m}}\right]^{\mathsf{T}}, \tag{8}$$

which depends on the coupler-position vector. The channel vector between all couplers and user $k$ is

$$\mathbf{h}_{\mathrm{C},k}(\mathbf{p}) = \sum_{\ell=1}^{L_k} \alpha_{k,\ell}\mathbf{a}_{\mathrm{C},k,\ell}(\mathbf{p}) \in \mathbb{C}^{MN\times 1}. \tag{9}$$

Based on (3) and (9), the overall multipath channel vector from the FCA array to user $k$ is given by

$$\mathbf{h}_k(\mathbf{p}) = \left[\mathbf{h}_{\mathrm{A},k}^{\mathrm{T}}, \mathbf{h}_{\mathrm{C},k}^{\mathrm{T}}(\mathbf{p})\right]^{\mathrm{T}} \in \mathbb{C}^{(MN+M)\times 1}, \tag{10}$$

which depends on coupler positions $\mathbf{p}$ while the active antenna positions are fixed. Collecting the channel vectors of all users

Authorized licensed use limited to: Nanjing University. Downloaded on October 30,2026 at 06:12:46 UTC from IEEE Xplore. Restrictions apply.

yields the following multiuser MIMO channel matrix

$$\mathbf{H}(\mathbf{p}) = [\mathbf{h}_1(\mathbf{p}), \ldots, \mathbf{h}_K(\mathbf{p})] \in \mathbb{C}^{(MN+M)\times K}. \tag{11}$$

### C. Mechanical Beamforming

Let $\mathbf{i}_{\mathrm{A}} \in \mathbb{C}^{M\times 1}$ denote the current vector of all active antennas, and $\mathbf{i}_{\mathrm{C}} \in \mathbb{C}^{MN\times 1}$ denote the current vector of all couplers. The current vector across all active antennas and couplers is given by

$$\mathbf{i} = \left[\mathbf{i}_{\mathrm{A}}^{\mathrm{T}}, \mathbf{i}_{\mathrm{C}}^{\mathrm{T}}\right]^{\mathrm{T}} \in \mathbb{C}^{(MN+M)\times 1}. \tag{12}$$

Similarly, let the active-antenna voltage vector be $\mathbf{v}_{\mathrm{A}} \in \mathbb{C}^{M\times 1}$ and the coupler voltage vector be $\mathbf{v}_{\mathrm{C}} \in \mathbb{C}^{MN\times 1}$. The voltage vector across all active antennas and couplers is given by

$$\mathbf{v} = \left[\mathbf{v}_{\mathrm{A}}^{\mathrm{T}}, \mathbf{v}_{\mathrm{C}}^{\mathrm{T}}\right]^{\mathrm{T}} \in \mathbb{C}^{(MN+M)\times 1}. \tag{13}$$

In general, the mutual impedance matrix between all couplers and all active antennas can be denoted by $\bar{\mathbf{Z}}(\mathbf{p}) \in \mathbb{C}^{MN\times M}$ [21]. We denote the mutual coupling vector between the $j$-th active antenna and the $N$ couplers associated with the $i$-th active antenna by $\bar{\mathbf{z}}_{i,j} \in \mathbb{C}^{N\times 1}$. Then, $\bar{\mathbf{Z}}(\mathbf{p})$ can be written as

$$\bar{\mathbf{Z}}(\mathbf{p}) = \begin{bmatrix} \bar{\mathbf{z}}_{1,1} & \cdots & \bar{\mathbf{z}}_{1,M} \\ \vdots & \ddots & \vdots \\ \bar{\mathbf{z}}_{M,1} & \cdots & \bar{\mathbf{z}}_{M,M} \end{bmatrix} \in \mathbb{C}^{MN\times M}. \tag{14}$$

Let $\widetilde{\mathbf{Z}} \in \mathbb{C}^{M\times M}$ denote the mutual impedance among all active antennas and $\hat{\mathbf{Z}}(\mathbf{p}) \in \mathbb{C}^{MN\times MN}$ denote the mutual impedance among all couplers. The overall mutual impedance matrix of the FCA array is thus given by

$$\mathbf{Z}(\mathbf{p}) = \begin{bmatrix} \widetilde{\mathbf{Z}} & \bar{\mathbf{Z}}^{\mathrm{T}}(\mathbf{p}) \\ \bar{\mathbf{Z}}(\mathbf{p}) & \hat{\mathbf{Z}}(\mathbf{p}) \end{bmatrix} \in \mathbb{C}^{(MN+M)\times(MN+M)}. \tag{15}$$

For practical implementation considerations, we assume that the active antennas are physically isolated by metallic plates. The center-to-center distance between any two active antennas is assumed to be significantly larger than the distance between each active antenna and its associated passive couplers, as well as the distances among the couplers themselves. Consequently, the mutual coupling between ports associated with different FCAs becomes negligible and can be ignored. Under this assumption, the overall mutual impedance matrix exhibits a block-diagonal structure. Accordingly, we define the mutual impedance submatrix corresponding to the $m$-th FCA as

$$\mathbf{Z}_m(\mathbf{p}_m) = \begin{bmatrix} \tilde{z}_m & \bar{\mathbf{Z}}_m^{\mathrm{T}}(\mathbf{p}_m) \\ \bar{\mathbf{z}}_m(\mathbf{p}_m) & \hat{\mathbf{Z}}_m(\mathbf{p}_m) \end{bmatrix} \in \mathbb{C}^{(N+1)\times(N+1)}, \tag{16}$$

where $\tilde{z}_m \in \mathbb{C}$ denotes the self-impedance of the $m$-th active antenna, $\bar{\mathbf{z}}_m(\mathbf{p}_m) \in \mathbb{C}^{N\times 1}$ collects the mutual impedances between this active antenna and its associated $N$ couplers, and $\hat{\mathbf{Z}}_m(\mathbf{p}_m) \in \mathbb{C}^{N\times N}$ denotes the mutual impedance matrix among these couplers.

The entries of the mutual impedance matrix $\mathbf{Z}_m(\mathbf{p}_m)$ in (16) are computed based on the thin-wire dipole model with element length $D$ and radius $a$. Let $\mathbf{p}_{0,m} \triangleq \mathbf{q}_m$ denote the position of the $m$-th active antenna. For $i \neq j$, $i, j \in \{0\} \cup \mathcal{N}$, $[\mathbf{Z}_m(\mathbf{p}_m)]_{i,j}$ depends on the center-to-center distance $d = \|\mathbf{p}_{i,m} - \mathbf{p}_{j,m}\|_2$, and its real and imaginary parts are given by $\Re\{[\mathbf{Z}_m(\mathbf{p}_m)]_{i,j}\} = \frac{\eta}{4\pi}[2\mathrm{Ci}(u_0) - \mathrm{Ci}(u_1) - \mathrm{Ci}(u_2)]$ and $\Im\{[\mathbf{Z}_m(\mathbf{p}_m)]_{i,j}\} = -\frac{\eta}{4\pi}[2\mathrm{Si}(u_0) - \mathrm{Si}(u_1) - \mathrm{Si}(u_2)]$, respectively, where $u_0 = \frac{2\pi d}{\lambda}$, $u_1 = \frac{2\pi}{\lambda}(\sqrt{d^2 + D^2} + D)$, $u_2 = \frac{2\pi}{\lambda}(\sqrt{d^2 + D^2} - D)$, $\mathrm{Si}(x) = \int_0^x \frac{\sin\tau}{\tau}\,\mathrm{d}\tau$, and $\mathrm{Ci}(x) = -\int_x^\infty \frac{\cos\tau}{\tau}\,\mathrm{d}\tau$. For $i = j$, $[\mathbf{Z}_m(\mathbf{p}_m)]_{i,i}$ is independent of the coupler positions and is computed using the closed-form self-impedance expressions with the parameter settings specified in Section V. Under the above block-diagonal assumption, the overall mutual impedance matrix can be simplified to

$$\mathbf{Z}(\mathbf{p}) = \mathrm{blkdiag}\left\{\mathbf{Z}_1(\mathbf{p}_1), \ldots, \mathbf{Z}_M(\mathbf{p}_M)\right\}. \tag{17}$$

Let $X_{n,m}$ denote the load impedance at the port of the $n$-th coupler associated with the $m$-th active antenna. The diagonal load-impedance matrix connected to the $N$ couplers of the $m$-th FCA is given by [21]

$$\mathbf{X}_m = \mathrm{diag}\{X_{1,m}, \ldots, X_{N,m}\} \in \mathbb{C}^{N\times N}. \tag{18}$$

Let $s \in \mathbb{C}$ denote the transmit information symbol with zero mean and unit variance. Antenna current vector $\mathbf{i}$ is adopted as the equivalent transmit precoding (beamforming) vector, such that the radiated signal is given by $\mathbf{i}s$. For the $m$-th FCA, define $\mathbf{v}_{\mathrm{C},m} \in \mathbb{C}^{N\times 1}$ as the port-voltage vector across the load impedances at the network side, and define the load-voltage drop along the direction of coupler current vector $\mathbf{i}_{\mathrm{C},m} \in \mathbb{C}^{N\times 1}$. By Kirchhoff's voltage law [22], we have

$$\mathbf{v}_{\mathrm{C},m} = -\mathbf{X}_m \mathbf{i}_{\mathrm{C},m}\, s, \quad m \in \mathcal{M}, \tag{19}$$

where $\mathcal{M} = \{1, 2, \ldots, M\}$. Moreover, the port voltages and currents of the linear multi-port network obey the impedance relation [23],

$$\mathbf{v} = \mathbf{Z}(\mathbf{p})\mathbf{i}s. \tag{20}$$

Partitioning (20) according to $\mathbf{v} = [\mathbf{v}_{\mathrm{A}}^{\mathrm{T}}, \mathbf{v}_{\mathrm{C}}^{\mathrm{T}}]^{\mathrm{T}}$ and $\mathbf{i} = [\mathbf{i}_{\mathrm{A}}^{\mathrm{T}}, \mathbf{i}_{\mathrm{C}}^{\mathrm{T}}]^{\mathrm{T}}$ and using (17) yield

$$\mathbf{v}_{\mathrm{C},m} = \bar{\mathbf{z}}_m(\mathbf{p}_m) i_{\mathrm{A},m} s + \hat{\mathbf{Z}}_m(\mathbf{p}_m)\mathbf{i}_{\mathrm{C},m} s,\ m \in \mathcal{M}, \tag{21}$$

where $i_{\mathrm{A},m}$ is the current at the $m$th active antenna, and $\mathbf{i}_{\mathrm{C},m} \in \mathbb{C}^{N\times 1}$ collects the currents of the associated $N$ couplers. Equating (19) and (21) gives

$$\begin{aligned} \mathbf{i}_{\mathrm{C},m} &= -\left(\hat{\mathbf{Z}}_m(\mathbf{p}_m) + \mathbf{X}_m\right)^{-1} \bar{\mathbf{z}}_m(\mathbf{p}_m) i_{\mathrm{A},m} \\ &= -\mathbf{w}_m(\mathbf{p}_m) i_{\mathrm{A},m}, \end{aligned} \tag{22}$$

where

$$\mathbf{w}_m(\mathbf{p}_m) = \left(\hat{\mathbf{Z}}_m(\mathbf{p}_m) + \mathbf{X}_m\right)^{-1} \bar{\mathbf{z}}_m(\mathbf{p}_m) \in \mathbb{C}^{N\times 1}, \tag{23}$$

is the local precoding/beamforming vector of the $m$-th FCA. We refer to $\mathbf{w}_m(\mathbf{p}_m)$ as the mechanical beamforming vector, since its beamforming weights can be reconfigured through adjusting the coupler positions, $\mathbf{p}_m$. Stacking the mechanical

Authorized licensed use limited to: Nanjing University. Downloaded on October 30,2026 at 06:12:46 UTC from IEEE Xplore. Restrictions apply.

beamforming vectors of all FCAs gives the following block-diagonal mechanical beamforming matrix,

$$\mathbf{W}(\mathbf{p}) = \text{blkdiag}\left\{\mathbf{w}_1(\mathbf{p}_1), \ldots, \mathbf{w}_M(\mathbf{p}_M)\right\} \in \mathbb{C}^{MN\times M}. \quad (24)$$

The matrix $\mathbf{W}(\mathbf{p})$ maps the active-antenna currents to the induced coupler currents through position-dependent electromagnetic coupling.

### D. Signal Model

For user $k \in \mathcal{K} = \{1, 2, \ldots, K\}$, let $s_k \in \mathbb{C}$ denote the transmit information symbol with $\mathbb{E}\{|s_k|^2\} = 1$. We collect all user symbols into the vector, $\mathbf{s} = [s_1, \ldots, s_K]^{\mathsf{T}} \in \mathbb{C}^{K\times 1}$, which satisfies $\mathbb{E}\{\mathbf{s}\mathbf{s}^{\mathsf{H}}\} = \mathbf{I}_K$.

For a given coupler-position vector $\mathbf{p}$, we use the active-antenna current vector as the equivalent digital beamforming vector across the $M$ FCAs. Specifically, for user $k \in \mathcal{K}$, we define

$$\mathbf{i}_{\mathrm{A},k} = [i_{\mathrm{A},1,k}, \ldots, i_{\mathrm{A},M,k}]^{\mathsf{T}} \in \mathbb{C}^{M\times 1}, \quad (25)$$

where $i_{\mathrm{A},m,k}$ is the current injected into the $m$-th active antenna for user $k$. Stacking $\{\mathbf{i}_{\mathrm{A},k}\}_{k=1}^{K}$ yields digital precoding matrix

$$\mathbf{U} = [\mathbf{i}_{\mathrm{A},1}, \ldots, \mathbf{i}_{\mathrm{A},K}] \in \mathbb{C}^{M\times K}. \quad (26)$$

Next, we absorb user symbols $\{s_k\}_{k=1}^{K}$ into the injected currents and obtain the instantaneous active-antenna current vector as

$$\mathbf{i}_{\mathrm{A}} = \sum_{k=1}^{K} \mathbf{i}_{\mathrm{A},k} s_k = \mathbf{U}\mathbf{s} \in \mathbb{C}^{M\times 1}, \quad (27)$$

which equivalently redefines the effective complex amplitude and phase of each symbol $s_k$. According to (22), the corresponding coupler current vector is given by

$$\mathbf{i}_{\mathrm{C}} = -\mathbf{W}(\mathbf{p})\mathbf{i}_{\mathrm{A}} = -\mathbf{W}(\mathbf{p})\mathbf{U}\mathbf{s} \in \mathbb{C}^{MN\times 1}. \quad (28)$$

Stacking the currents of all active antennas and all couplers yields the instantaneous port current vector

$$\mathbf{i}_{\text{tot}} = \left[\mathbf{i}_{\mathrm{A}}^{\mathrm{T}},\ \mathbf{i}_{\mathrm{C}}^{\mathrm{T}}\right]^{\mathrm{T}} = \left[\mathbf{I}_M, -\mathbf{W}(\mathbf{p})^{\mathrm{T}}\right]^{\mathrm{T}} \mathbf{U}\mathbf{s} = \widetilde{\mathbf{W}}(\mathbf{p})\mathbf{U}\mathbf{s}, \quad (29)$$

where

$$\widetilde{\mathbf{W}}(\mathbf{p}) = \left[\mathbf{I}_M,\ -\mathbf{W}(\mathbf{p})^{\mathrm{T}}\right]^{\mathrm{T}} \in \mathbb{C}^{(M+MN)\times M}, \quad (30)$$

denotes the overall mechanical beamforming matrix.

Then, the received signal at user $k$ is given by

$$y_k = \mathbf{h}_k^{\mathsf{T}}(\mathbf{p})\, \mathbf{i}_{\text{tot}} + n_k \quad (31a)$$

$$= \mathbf{h}_k^{\mathsf{T}}(\mathbf{p})\, \widetilde{\mathbf{W}}(\mathbf{p})\mathbf{U}\mathbf{s} + n_k \quad (31b)$$

$$= \mathbf{h}_k^{\mathsf{T}}(\mathbf{p})\, \widetilde{\mathbf{W}}(\mathbf{p})\mathbf{i}_{\mathrm{A},k} s_k + \sum_{j\in\mathcal{K},\, j\neq k} \mathbf{h}_k^{\mathsf{T}}(\mathbf{p})\, \widetilde{\mathbf{W}}(\mathbf{p})\mathbf{i}_{\mathrm{A},j} s_j + n_k, \quad (31c)$$

where $n_k \sim \mathcal{CN}(0, \sigma_k^2)$ denotes receive complex additive Gaussian noise at user $k$ with zero mean and variance $\sigma_k^2$. Thus, $\mathbf{h}_k(\mathbf{p})$ and $\widetilde{\mathbf{W}}(\mathbf{p})$ jointly determine the effective channel of user $k$.

Then, the signal-to-interference-plus-noise ratio (SINR) for decoding $s_k$ at user $k$ is given by

$$\gamma_k(\mathbf{p}, \mathbf{U}) = \frac{\left|\mathbf{h}_k^{\mathsf{T}}(\mathbf{p})\, \widetilde{\mathbf{W}}(\mathbf{p})\mathbf{i}_{\mathrm{A},k}\right|^2}{\sum_{j\in\mathcal{K},\, j\neq k} \left|\mathbf{h}_k^{\mathsf{T}}(\mathbf{p})\, \widetilde{\mathbf{W}}(\mathbf{p})\mathbf{i}_{\mathrm{A},j}\right|^2 + \sigma_k^2}. \quad (32)$$

Accordingly, the achievable downlink sum rate per hertz is given by

$$R(\mathbf{p}, \mathbf{U}) = \sum_{k=1}^{K} \log_2\left(1 + \gamma_k(\mathbf{p}, \mathbf{U})\right). \quad (33)$$

## III. Optimization of Coupler Positions

### A. Problem Formulation

According to multiport circuit theory [23], the average transmit power equals the expected real power

$$P = \mathbb{E}\left\{\Re\left\{\mathbf{i}_{\text{tot}}^{\mathsf{H}}\, \mathbf{v}_{\text{tot}}\right\}\right\}, \quad (34)$$

where the expectation is taken over the random information symbols involved in $\mathbf{i}_{\text{tot}}$. Using the impedance relation $\mathbf{v}_{\text{tot}} = \mathbf{Z}(\mathbf{p})\mathbf{i}_{\text{tot}}$, we obtain

$$P = \mathbb{E}\left\{\mathbf{i}_{\text{tot}}^{\mathsf{H}}\, \Re\{\mathbf{Z}(\mathbf{p})\}\, \mathbf{i}_{\text{tot}}\right\}$$

$$= \mathbb{E}\left\{\mathbf{s}^{\mathsf{H}}\mathbf{U}^{\mathsf{H}}\widetilde{\mathbf{W}}^{\mathsf{H}}(\mathbf{p})\, \Re\{\mathbf{Z}(\mathbf{p})\}\, \widetilde{\mathbf{W}}(\mathbf{p})\mathbf{U}\mathbf{s}\right\}. \quad (35)$$

With $\mathbb{E}\{\mathbf{s}\mathbf{s}^{\mathsf{H}}\} = \mathbf{I}_K$, the transmit power simplifies to

$$P = \text{tr}\left(\mathbf{U}^{\mathsf{H}}\mathbf{B}(\mathbf{p})\mathbf{U}\right), \quad (36)$$

where

$$\mathbf{B}(\mathbf{p}) = \widetilde{\mathbf{W}}^{\mathsf{H}}(\mathbf{p})\, \Re\{\mathbf{Z}(\mathbf{p})\}\, \widetilde{\mathbf{W}}(\mathbf{p}) \quad (37)$$

is positive semidefinite and captures the effects of mutual coupling and the movement configuration on the power consumption.

Under the block-diagonal structure in (17) and the local mechanical beamforming vectors in (22), $\mathbf{B}(\mathbf{p})$ takes the following diagonal form,

$$\mathbf{B}(\mathbf{p}) = \text{diag}\left\{b_1(\mathbf{p}_1), \ldots, b_M(\mathbf{p}_M)\right\}, \quad (38)$$

where

$$b_m(\mathbf{p}_m) = \widetilde{\mathbf{w}}_m^{\mathsf{H}}(\mathbf{p}_m)\, \Re\{\mathbf{Z}_m(\mathbf{p}_m)\}\, \widetilde{\mathbf{w}}_m(\mathbf{p}_m), \quad (39)$$

with $\widetilde{\mathbf{w}}_m(\mathbf{p}_m) = [1,\ -\mathbf{w}_m^{\mathsf{T}}(\mathbf{p}_m)]^{\mathsf{T}} \in \mathbb{C}^{(N+1)\times 1}$.

Let $P_{\max}$ denote the maximum available transmit power. The transmit power constraint is given by

$$\text{tr}\left(\mathbf{U}^{\mathsf{H}}\mathbf{B}(\mathbf{p})\mathbf{U}\right) \le P_{\max}. \quad (40)$$

We aim to jointly optimize the coupler positions and the digital beamforming matrix to maximize the achievable sum rate, subject to the transmit power constraint and the movement constraints. The problem is formulated as

$$(\mathrm{P1}) \max_{\{\mathbf{p}_m\}_{m=1}^{M},\, \mathbf{U}} \quad R(\mathbf{p}, \mathbf{U}) \quad (41a)$$

$$\text{s.t. } \text{tr}\left(\mathbf{U}^{\mathsf{H}}\mathbf{B}(\mathbf{p})\mathbf{U}\right) \le P_{\max}, \quad (41b)$$

$$\mathbf{p}_{n,m} \in \mathcal{C}_m, \forall n \in \mathcal{N}, \forall m \in \mathcal{M}, \quad (41c)$$

Authorized licensed use limited to: Nanjing University. Downloaded on October 30,2026 at 06:12:46 UTC from IEEE Xplore. Restrictions apply.

$$\|\mathbf{p}_{n,m}-\mathbf{p}_{n',m}\|_2 \geq d_{\min}, \forall n,n' \in \{0\}\cup\mathcal{N}, \quad n\neq n', m\in\mathcal{M}, \tag{41d}$$

where $\mathcal{N}=\{1,2,\ldots,N\}$ and $\mathbf{p}_{0,m} \triangleq \mathbf{q}_m$ denotes the location of the $m$th active antenna. Problem (P1) is nonconvex because the sum rate in (41a) is nonconcave with respect to $(\mathbf{p},\mathbf{U})$ and the spacing constraints in (41d) are nonconvex. In the following, we first derive a closed-form MMSE-based digital precoder for given coupler positions, and then reduce (P1) to a position-only problem that is amenable to distributed optimization.

### B. MMSE-Based Digital Beamforming

For fixed coupler positions $\mathbf{p}$, the received signal at user $k$ can be written as

$$y_k = \mathbf{g}_k^{\mathsf{H}}(\mathbf{p})\mathbf{U}\mathbf{s}+n_k, \tag{42}$$

where the effective channel after mechanical beamforming is

$$\mathbf{g}_k^{\mathsf{H}}(\mathbf{p}) = \mathbf{h}_k^{\mathsf{T}}(\mathbf{p})\,\widetilde{\mathbf{W}}(\mathbf{p}) \in \mathbb{C}^{1\times M}, \tag{43}$$

and the effective channel matrix is given by

$$\mathbf{G}(\mathbf{p}) = [\mathbf{g}_1(\mathbf{p}),\ldots,\mathbf{g}_K(\mathbf{p})]^{\mathsf{T}} \in \mathbb{C}^{K\times M}. \tag{44}$$

Using the diagonal structure of $\mathbf{B}(\mathbf{p})$ in (38), we introduce the whitened precoder

$$\mathbf{F} = \mathbf{B}^{1/2}(\mathbf{p})\mathbf{U} \in \mathbb{C}^{M\times K}, \tag{45}$$

with

$$\mathbf{B}^{1/2}(\mathbf{p}) = \operatorname{diag}\left\{\sqrt{b_1(\mathbf{p}_1)},\ldots,\sqrt{b_M(\mathbf{p}_M)}\right\}. \tag{46}$$

Then, we have $\mathbf{U}=\mathbf{B}^{-1/2}(\mathbf{p})\mathbf{F}$, and the transmit power constraint (36) is equivalent to

$$\|\mathbf{F}\|_F^2 \leq P_{\max}. \tag{47}$$

Substituting $\mathbf{U}=\mathbf{B}^{-1/2}(\mathbf{p})\mathbf{F}$ into (42) yields

$$y_k = \overline{\mathbf{g}}_k^{\mathsf{H}}(\mathbf{p})\mathbf{F}\mathbf{s}+n_k, \tag{48}$$

where $\overline{\mathbf{g}}_k^{\mathsf{H}}(\mathbf{p}) = \mathbf{g}_k^{\mathsf{H}}(\mathbf{p})\,\mathbf{B}^{-1/2}(\mathbf{p})$.

For given coupler positions $\mathbf{p}$, the FCA system reduces to a conventional downlink multiuser MIMO with precoder $\mathbf{F}$ under (47) and effective channel matrix

$$\overline{\mathbf{G}}(\mathbf{p}) = [\overline{\mathbf{g}}_1(\mathbf{p}),\ldots,\overline{\mathbf{g}}_K(\mathbf{p})]^{\mathsf{T}} = \mathbf{G}(\mathbf{p})\mathbf{B}^{-1/2}(\mathbf{p}). \tag{49}$$

We obtain $\mathbf{F}$ by solving the regularized least-square (LS) problem

$$\min_{\mathbf{F}} \left\|\overline{\mathbf{G}}(\mathbf{p})\mathbf{F}-\mathbf{I}_K\right\|_F^2 + \alpha\|\mathbf{F}\|_F^2, \tag{50}$$

whose solution satisfies

$$\widehat{\mathbf{F}}_{\mathrm{MMSE}}(\mathbf{p}) = \overline{\mathbf{G}}^{\mathsf{H}}(\mathbf{p})\left(\overline{\mathbf{G}}(\mathbf{p})\overline{\mathbf{G}}^{\mathsf{H}}(\mathbf{p})+\alpha\mathbf{I}_K\right)^{-1}. \tag{51}$$

where $\alpha = K\sigma^2/P_{\max}$ [24]. To enforce (47) with equality, we further apply a scalar power loading factor

$$\beta(\mathbf{p}) = \sqrt{\frac{P_{\max}}{\left\|\widehat{\mathbf{F}}_{\mathrm{MMSE}}(\mathbf{p})\right\|_F^2}}, \tag{52}$$

and set $\mathbf{F}_{\mathrm{MMSE}}(\mathbf{p}) = \beta(\mathbf{p})\widehat{\mathbf{F}}_{\mathrm{MMSE}}(\mathbf{p})$. Therefore, the MMSE-based digital precoder is given by

$$\mathbf{U}_{\mathrm{MMSE}}(\mathbf{p}) = \mathbf{B}^{-1/2}(\mathbf{p})\,\mathbf{F}_{\mathrm{MMSE}}(\mathbf{p}) \in \mathbb{C}^{M\times K}. \tag{53}$$

This construction guarantees

$$\operatorname{tr}\left(\mathbf{U}_{\mathrm{MMSE}}^{\mathsf{H}}\mathbf{B}(\mathbf{p})\mathbf{U}_{\mathrm{MMSE}}\right) = \|\mathbf{F}_{\mathrm{MMSE}}(\mathbf{p})\|_F^2 = P_{\max}. \tag{54}$$

### C. Coupler Position Optimization Algorithm

Since the MMSE-based digital precoder $\mathbf{U}_{\mathrm{MMSE}}(\mathbf{p})$ is available in closed form for any given $\mathbf{p}$ and already satisfies the power constraint in (41b), we eliminate $\mathbf{U}$ from problem (P1). Specifically, by substituting $\mathbf{U}=\mathbf{U}_{\mathrm{MMSE}}(\mathbf{p})$ into (32), the SINR of user $k$ becomes

$$\gamma_k^{\mathrm{MMSE}}(\mathbf{p}) = \frac{\left|\mathbf{h}_k^{\mathsf{T}}(\mathbf{p})\,\widetilde{\mathbf{W}}(\mathbf{p})\,\mathbf{u}_k^{\mathrm{MMSE}}(\mathbf{p})\right|^2}{\sum\limits_{j\in\mathcal{K},\,j\neq k}\left|\mathbf{h}_k^{\mathsf{T}}(\mathbf{p})\,\widetilde{\mathbf{W}}(\mathbf{p})\,\mathbf{u}_j^{\mathrm{MMSE}}(\mathbf{p})\right|^2+\sigma_k^2}, \tag{55}$$

where $\mathbf{u}_k^{\mathrm{MMSE}}(\mathbf{p})$ is the $k$-th column of $\mathbf{U}_{\mathrm{MMSE}}(\mathbf{p})$. The corresponding achievable sum rate is

$$R_{\mathrm{MMSE}}(\mathbf{p}) = \sum_{k=1}^{K}\log_2\left(1+\gamma_k^{\mathrm{MMSE}}(\mathbf{p})\right). \tag{56}$$

This leads to the following position-only optimization problem,

$$(\mathrm{P2}) \max_{\{\mathbf{p}_m\}_{m=1}^M} \quad R_{\mathrm{MMSE}}(\mathbf{p}) \tag{57a}$$

$$\text{s.t. } (41c),(41d). \tag{57b}$$

Problem (P2) is still nonconvex due to the complicated dependence of $R_{\mathrm{MMSE}}(\mathbf{p})$ on $\mathbf{p}$ and the nonconvex spacing constraints in (41d). However, the two constraints (41c) and (41d) are separable across different FCAs, which enables a distributed optimization algorithm.

Let

$$\mathcal{S}_m = \left\{\mathbf{p}_m \,\middle|\, \mathbf{p}_{n,m}\in\mathcal{C}_m,\ \|\mathbf{p}_{n,m}-\mathbf{p}_{n',m}\|_2\geq d_{\min}, \forall n,n'\in\{0\}\cup\mathcal{N},\ n\neq n'\right\}, \tag{58}$$

denote the local feasible set of coupler positions at the $m$-th FCA. Due to the spacing constraints, $\mathcal{S}_m$ is in general nonconvex. To apply the SCA framework with convergence guarantees, we construct at each iteration a convex inner approximation of $\mathcal{S}_m$. Specifically, for each pair $(n,n')$ with $n\neq n'$, we define

$$d_{n,n',m}(\mathbf{p}_m) = \left\|\mathbf{p}_{n,m}-\mathbf{p}_{n',m}\right\|_2^2, \tag{59}$$

so that the spacing constraint is equivalent to $-d_{n,n',m}(\mathbf{p}_m)\leq -d_{\min}^2$. Since $-d_{n,n',m}(\mathbf{p}_m)$ is concave, its first-order Taylor approximation at $\mathbf{p}_m^{(t)}$ yields a global affine upper bound. Denote

$$\widetilde{d}_{n,n',m}(\mathbf{p}_m;\mathbf{p}_m^{(t)}) = -d_{n,n',m}(\mathbf{p}_m^{(t)}) - \nabla_{\mathbf{p}_m} d_{n,n',m}(\mathbf{p}_m^{(t)})^{\mathsf{T}}\left(\mathbf{p}_m-\mathbf{p}_m^{(t)}\right), \tag{60}$$

Authorized licensed use limited to: Nanjing University. Downloaded on October 30,2026 at 06:12:46 UTC from IEEE Xplore. Restrictions apply.

where the gradient can be obtained in closed form. At iteration $t$, we approximate the spacing constraint by

$$\widetilde{d}_{n,n',m}(\mathbf{p}_m;\mathbf{p}_m^{(t)}) \le -d_{\min}^2, \forall n \ne n',\ n,n' \in \{0\}\cup\mathcal{N}. \quad (61)$$

The resulting convex inner approximation of $\mathcal{S}_m$ is

$$\mathcal{S}_m^{(t)} = \Big\{\mathbf{p}_m \,\Big|\, \mathbf{p}_{n,m} \in \mathcal{C}_m,\ \widetilde{d}_{n,n',m}(\mathbf{p}_m;\mathbf{p}_m^{(t)}) \le -d_{\min}^2, \forall n,n' \in \{0\}\cup\mathcal{N},\ n \ne n'\Big\}, \quad (62)$$

which satisfies $\mathcal{S}_m^{(t)} \subseteq \mathcal{S}_m$ for all $t$.

For problem (P2), the feasible set is separable across the $M$ FCAs through $\{\mathcal{S}_m\}_{m=1}^M$, while the objective function $R_{\mathrm{MMSE}}(\mathbf{p})$ couples all antennas through the effective channels and the MMSE-based digital precoder. Let

$$J(\mathbf{p}) = R_{\mathrm{MMSE}}(\mathbf{p}) \quad (63)$$

denote the sum-rate objective in (P2). Given $\mathbf{p}^{(t)}$ at iteration $t$, we consider a first-order approximation of $J(\mathbf{p})$ with respect to $\mathbf{p}_m$ around $\mathbf{p}_m^{(t)}$, and add a quadratic regularization term. For each $m \in \mathcal{M}$, we define the local surrogate function as

$$\widetilde{J}_m(\mathbf{p}_m;\mathbf{p}^{(t)}) = J(\mathbf{p}^{(t)}) + \left(\nabla_{\mathbf{p}_m} J(\mathbf{p}^{(t)})\right)^{\mathsf{T}} \left(\mathbf{p}_m - \mathbf{p}_m^{(t)}\right) - \frac{\eta_m}{2}\left\|\mathbf{p}_m - \mathbf{p}_m^{(t)}\right\|_2^2, \quad (64)$$

where $\eta_m > 0$ is a design parameter no smaller than the Lipschitz constant of $\nabla_{\mathbf{p}_m} J(\mathbf{p})$ to ensure monotonic improvement.

The gradient of the sum rate with respect to $\mathbf{p}_m$ is denoted by

$$\mathbf{g}_m(\mathbf{p}) = \nabla_{\mathbf{p}_m} J(\mathbf{p}) \in \mathbb{R}^{2N}, \quad (65)$$

which can be obtained by applying the chain rule to (56).

For fixed $\mathbf{p}^{(t)}$ and each $m$, we consider the following local strongly concave maximization problem

$$\text{(P3-m)} \max_{\mathbf{p}_m} \quad \widetilde{J}_m(\mathbf{p}_m;\mathbf{p}^{(t)}) \quad (66a)$$

$$\text{s.t.} \quad \mathbf{p}_m \in \mathcal{S}_m^{(t)}. \quad (66b)$$

By substituting (65) into (64) and dropping the constant term $J(\mathbf{p}^{(t)})$, (P3-$m$) is equivalent to

$$\max_{\mathbf{p}_m \in \mathcal{S}_m^{(t)}} \ \mathbf{g}_m^{\mathsf{T}}(\mathbf{p}^{(t)}) \left(\mathbf{p}_m - \mathbf{p}_m^{(t)}\right) - \frac{\eta_m}{2}\left\|\mathbf{p}_m - \mathbf{p}_m^{(t)}\right\|_2^2. \quad (67)$$

Ignoring the constraint in (67) yields the following unconstrained maximizer

$$\mathbf{p}_m^{\mathrm{uncon}} = \mathbf{p}_m^{(t)} + \frac{1}{\eta_m}\mathbf{g}_m(\mathbf{p}^{(t)}). \quad (68)$$

Then, the solution of (P3-$m$) is obtained by projecting $\mathbf{p}_m^{\mathrm{uncon}}$ onto $\mathcal{S}_m^{(t)}$,

$$\widehat{\mathbf{p}}_m^{(t+1)} = \mathcal{P}_{\mathcal{S}_m^{(t)}}\left(\mathbf{p}_m^{(t)} + \tfrac{1}{\eta_m}\mathbf{g}_m(\mathbf{p}^{(t)})\right), \quad (69)$$

where $\mathcal{P}_{\mathcal{S}_m^{(t)}}(\cdot)$ denotes the Euclidean projection onto $\mathcal{S}_m^{(t)}$. This projection can be performed locally by enforcing (41c) and the linearized spacing constraints.

**Algorithm 1:** Distributed Coupler Position Optimization Algorithm.

1: **Input:** $P_{\max}$, $\{\mathcal{C}_m\}_{m=1}^M$, $d_{\min}$, $\{\eta_m\}_{m=1}^M$, $\{\alpha_m^{(t)}\}$, tolerance $\varepsilon > 0$.
2: **Initialization:** Choose a feasible $\mathbf{p}^{(0)}$ satisfying (41c)–(41d); set $t = 0$.
3: CPU computes $\overline{\mathbf{G}}(\mathbf{p}^{(0)})$ and $\mathbf{U}_{\mathrm{MMSE}}(\mathbf{p}^{(0)})$ according to (51)–(53), and evaluates $R^{(0)} = R_{\mathrm{MMSE}}(\mathbf{p}^{(0)})$.
4: **repeat**
5: CPU computes $\mathbf{g}_m(\mathbf{p}^{(t)})$ for all $m \in \mathcal{M}$ and broadcasts $\{\mathbf{g}_m(\mathbf{p}^{(t)})\}_{m=1}^M$.
6: **for** $m = 1$ to $M$ **(in parallel) do**
7: $\mathbf{p}_m^{\mathrm{uncon}} = \mathbf{p}_m^{(t)} + \frac{1}{\eta_m}\mathbf{g}_m(\mathbf{p}^{(t)})$.
8: $\widehat{\mathbf{p}}_m^{(t+1)} = \mathcal{P}_{\mathcal{S}_m^{(t)}}(\mathbf{p}_m^{\mathrm{uncon}})$ via (69).
9: Update $\mathbf{p}_m^{(t+1)}$ via (70).
10: **end for**
11: CPU forms $\mathbf{p}^{(t+1)}$ by stacking $\{\mathbf{p}_m^{(t+1)}\}_{m=1}^M$.
12: CPU recomputes $\overline{\mathbf{G}}(\mathbf{p}^{(t+1)})$ and updates $\mathbf{U}_{\mathrm{MMSE}}(\mathbf{p}^{(t+1)})$ according to (51)–(53).
13: CPU evaluates $R^{(t+1)} = R_{\mathrm{MMSE}}(\mathbf{p}^{(t+1)})$ via (56).
14: $t \leftarrow t+1$.
15: **until** $\left|R^{(t)} - R^{(t-1)}\right| / R^{(t-1)} \le \varepsilon$
16: **Output:** $\mathbf{p}^\star = \mathbf{p}^{(t)}$ and $\mathbf{U}_{\mathrm{MMSE}}^\star = \mathbf{U}_{\mathrm{MMSE}}(\mathbf{p}^\star)$.

To further improve robustness, we adopt the relaxation step

$$\mathbf{p}_m^{(t+1)} = \mathbf{p}_m^{(t)} + \alpha_m^{(t)}\left(\widehat{\mathbf{p}}_m^{(t+1)} - \mathbf{p}_m^{(t)}\right), \quad (70)$$

where $\alpha_m^{(t)} \in (0,1]$ satisfies standard diminishing conditions, i.e., $\sum_t \alpha_m^{(t)} = \infty$ and $\sum_t (\alpha_m^{(t)})^2 < \infty$ [25].

Algorithm 1 summarizes the distributed coupler position optimization procedure based on a distributed SCA scheme, where each FCA maximizes a strongly concave local surrogate of the global sum rate. Under standard smoothness assumptions on $J(\mathbf{p})$ and a diminishing step size sequence, the generated sequence $\{\mathbf{p}^{(t)}\}$ yields nondecreasing sum rate $J(\mathbf{p}^{(t)})$, and every limit point of $\{\mathbf{p}^{(t)}\}$ is a stationary solution of problem (P2). The per-iteration computational complexity is dominated by the computation of the MMSE-based precoder and the gradients, and is given by $\mathcal{O}(K^2M + K^3 + KMN + MN^2)$. Let $T_{\max}$ denote the number of iterations required by the stopping criterion in Algorithm 1. The overall complexity therefore scales as $\mathcal{O}(T_{\max}(K^2M + K^3 + KMN + MN^2))$. At each iteration, the CPU broadcasts the local gradients to all LPUs, and each LPU uploads its updated coupler-position vector to the CPU. Hence, the communication overhead scales on the order of $MN$ scalar parameters.

## IV. Channel Estimation for Flexible Coupler Antenna Systems

As shown in Fig. 2, we propose a channel estimation protocol for FCA systems. Specifically, the channel training length $T_c$ (in time slots) is divided into $V$ pilot blocks indexed by $v \in \{1,\ldots,V\}$. At pilot block $v$, the $m$-th FCA sets the positions of

Authorized licensed use limited to: Nanjing University. Downloaded on October 30,2026 at 06:12:46 UTC from IEEE Xplore. Restrictions apply.

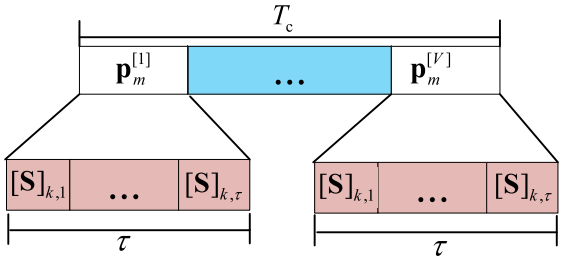



Fig. 2. Structured pilot pattern in the time domain.

its associated $N$ couplers to $\mathbf{p}_m^{[v]}$. We assume that all user channels remain constant over $T_c = V\tau$, where $\tau$ denotes the number of time slots in each pilot block. Therefore, the coupler position vector $\mathbf{p}_m^{[v]}$ remains unchanged during the $\tau$ time slots of the $v$-th block, and it varies across different blocks. This assumption is primarily intended for slowly time-varying scenarios. In high-mobility cases, it may be more practical to estimate statistical CSI for slower-timescale coupler-position optimization. Each user transmits a known pilot sequence $[\mathbf{S}]_{k,:} \in \mathbb{C}^{1\times\tau}$ to the BS, and the same pilot is repeated over the $V$ blocks. Let pilot matrix $\mathbf{S} \in \mathbb{C}^{K\times\tau}$ satisfy $\mathbf{S}\mathbf{S}^{\mathsf{H}} = \tau\mathbf{I}_K$.

Based on the proposed protocol, we first develop a pilot-assisted centralized channel estimation algorithm with high estimation accuracy and then present a pilot-assisted distributed channel estimation algorithm for FCA systems.

### A. Centralized Channel Estimation

First, we introduce the centralized channel estimation algorithm. Let

$$\mathbf{h}_{m,k}(\mathbf{p}_m^{[v]}) = \begin{bmatrix} [\mathbf{h}_{\mathrm{A},k}]_m \\ \mathbf{h}_{\mathrm{C},k}(\mathbf{p}_m^{[v]}) \end{bmatrix} \in \mathbb{C}^{(N+1)\times 1}, \tag{71}$$

denote the local channel from user $k$ to the $m$-th FCA under coupler position $\mathbf{p}_m^{[v]}$, where $\mathbf{h}_{\mathrm{C},k}(\mathbf{p}_m^{[v]}) = \sum_{\ell=1}^{L_k} \alpha_{k,\ell}\mathbf{a}_{\mathrm{C},k,\ell}(\mathbf{p}_m^{[v]}) \in \mathbb{C}^{N\times 1}$ collects the $N$ coupler to user-$k$ channels associated with $\mathbf{p}_m^{[v]}$. Under the proposed pilot pattern, the received signal at the $m$-th FCA is given by

$$\mathbf{y}_m^{[v]} = \widetilde{\mathbf{w}}_m^{\mathsf{T}}(\mathbf{p}_m^{[v]})\mathbf{H}_m(\mathbf{p}_m^{[v]})\mathbf{S} + \mathbf{n}_m^{[v]} \in \mathbb{C}^{1\times\tau}, \tag{72}$$

where $\mathbf{H}_m(\mathbf{p}_m^{[v]}) = [\mathbf{h}_{m,1}(\mathbf{p}_m^{[v]}), \ldots, \mathbf{h}_{m,K}(\mathbf{p}_m^{[v]})] \in \mathbb{C}^{(N+1)\times K}$ denotes the channel matrix between the $m$-th FCA and the users, and $\mathbf{n}_m^{[v]} \in \mathbb{C}^{1\times\tau}$ is the received Gaussian noise vector.

In the centralized channel estimation scheme, for each pilot block $v$, every FCA sends its received signal $\mathbf{y}_m^{[v]}$ to the CPU. The CPU stacks the received pilots across the $M$ antennas as

$$\mathbf{Y}^{[v]} = \left[(\mathbf{y}_1^{[v]})^{\mathsf{T}}, \ldots, (\mathbf{y}_M^{[v]})^{\mathsf{T}}\right]^{\mathsf{T}} \in \mathbb{C}^{M\times\tau}. \tag{73}$$

Based on (73), the CPU performs pilot correlation as

$$\widehat{\mathbf{G}}^{[v]} = \frac{1}{\tau}\mathbf{Y}^{[v]}\mathbf{S}^{\mathsf{H}}. \tag{74}$$

Consequently, for each user $k$, we obtain the stacked effective channel observation vector as

$$\widehat{\mathbf{y}}_k = \left[(\widehat{\mathbf{g}}_k^{[1]})^{\mathsf{T}}, \ldots, (\widehat{\mathbf{g}}_k^{[V]})^{\mathsf{T}}\right]^{\mathsf{T}} \in \mathbb{C}^{MV\times 1}, \tag{75}$$

where $\widehat{\mathbf{g}}_k^{[v]} = [\widehat{\mathbf{G}}^{[v]}]_{:,k} \in \mathbb{C}^{M\times 1}$.

Moreover, according to (10), the effective channel from user $k$ to the $m$-th FCA at signal block $v$ can be written as

$$g_{m,k}(\mathbf{p}_m^{[v]}) = \widetilde{\mathbf{w}}_m^{\mathsf{T}}(\mathbf{p}_m^{[v]})\mathbf{h}_{m,k}(\mathbf{p}_m^{[v]}) \tag{76a}$$

$$= \sum_{\ell=1}^{L_k} \alpha_{k,\ell}\, b_m(\phi_{k,\ell}; \mathbf{p}_m^{[v]}), \tag{76b}$$

where

$$b_m(\phi_{k,\ell}; \mathbf{p}_m^{[v]}) = [\mathbf{a}_y(\phi_{k,\ell})]_m - \mathbf{w}_m^{\mathsf{T}}(\mathbf{p}_m^{[v]})\,\mathbf{a}_{\mathrm{C},k,\ell}(\phi_{k,\ell}; \mathbf{p}_m^{[v]}). \tag{77}$$

To efficiently estimate $\{\alpha_{k,\ell}\}$ via compressed sensing, we approximate the azimuth domain by a uniform grid $\mathcal{G} = \{\phi_1, \ldots, \phi_G\}$, where $G \gg L_k$ denotes the number of grid points. For candidate angle $\phi$ and pilot block $v$, we define

$$\mathbf{b}(\phi; \mathbf{p}^{[v]}) = \left[b_1(\phi; \mathbf{p}_1^{[v]}), \ldots, b_M(\phi; \mathbf{p}_M^{[v]})\right]^{\mathsf{T}} \in \mathbb{C}^{M\times 1}, \tag{78}$$

where $\mathbf{p}^{[v]} = \{\mathbf{p}_m^{[v]}\}_{m=1}^M$. Then, the dictionary is constructed as

$$\mathbf{A} = [\mathbf{a}(\phi_1), \ldots, \mathbf{a}(\phi_G)] \in \mathbb{C}^{MV\times G}, \tag{79}$$

where

$$\mathbf{a}(\phi) = \left[\mathbf{b}(\phi; \mathbf{p}^{[1]})^{\mathsf{T}}, \ldots, \mathbf{b}(\phi; \mathbf{p}^{[V]})^{\mathsf{T}}\right]^{\mathsf{T}} \in \mathbb{C}^{MV\times 1}. \tag{80}$$

Since $\mathbf{S}\mathbf{S}^{\mathsf{H}} = \tau\mathbf{I}_K$, for each user $k$, the stacked observation in (75) can be expressed as the following sparse signal model

$$\widehat{\mathbf{y}}_k = \mathbf{A}\mathbf{x}_k + \widetilde{\mathbf{n}}_k, \tag{81}$$

where $\widetilde{\mathbf{n}}_k$ denotes the received Gaussian noise vector, $\mathbf{x}_k \in \mathbb{C}^{G\times 1}$ is $L_k$ sparse with $L_k$ nonzero elements that correspond to the $L_k$ propagation paths between user $k$ and the BS. In particular, the support of $\mathbf{x}_k$ specifies the $L_k$ grid indices that approximate azimuth angles $\{\phi_{k,\ell}\}_{\ell=1}^{L_k}$, and the associated nonzero coefficients represent the corresponding path gains.

Using orthogonal matching pursuit (OMP) [26], we perform exactly $L_k$ selections and obtain the support set, denoted by $\widehat{\Omega}_k = \{\widehat{\jmath}_{k,1}, \ldots, \widehat{\jmath}_{k,L_k}\}$. The estimated angles are obtained by mapping the selected indices to the predefined grid as

$$\widehat{\phi}_{k,\ell} = \phi_{\widehat{\jmath}_{k,\ell}}, \ell = 1, \ldots, L_k. \tag{82}$$

After obtaining $\widehat{\phi}_{k,\ell}$, we estimate the path gains using the LS technique, the resulting solution is given by

$$\widehat{\boldsymbol{\alpha}}_k = (\mathbf{A}_k^{\mathsf{H}}\mathbf{A}_k)^{-1}\mathbf{A}_k^{\mathsf{H}}\widehat{\mathbf{y}}_k \in \mathbb{C}^{L_k\times 1}, \tag{83}$$

where

$$\mathbf{A}_k = \left[\mathbf{a}(\widehat{\phi}_{k,1}), \ldots, \mathbf{a}(\widehat{\phi}_{k,L_k})\right] \in \mathbb{C}^{MV\times L_k}. \tag{84}$$

Authorized licensed use limited to: Nanjing University. Downloaded on October 30,2026 at 06:12:46 UTC from IEEE Xplore. Restrictions apply.

**Algorithm 2:** Centralized Channel Estimation for FCA system.

**Input S**, $\tau$, $\mathcal{G}$, $\{L_k\}_{k=1}^K$, $\{\mathbf{p}_m^{[v]}\}_{m=1,v=1}^{M,V}$.
**for** $v = 1$ to $V$ **do**
  Each FCA $m$ applies $\mathbf{p}_m^{[v]}$ and receives $\mathbf{y}_m^{[v]}$ in (72).
  Each FCA $m$ uploads $\mathbf{y}_m^{[v]}$ to the CPU.
  The CPU forms $\mathbf{Y}^{[v]}$ in (73) and computes $\widehat{\mathbf{G}}^{[v]}$ in (74).
**end for**
The CPU builds the dictionary $\mathbf{A}$ in (79) using (78).
**for** each user $k$ at the CPU **do**
  Form $\widehat{\mathbf{y}}_k$ in (75).
  Run OMP on (81) with $L_k$ selections and obtain $\widetilde{\Omega}_k$.
  Obtain $\{\widehat{\phi}_{k,\ell}\}_{\ell=1}^{L_k}$ by (82).
  Compute $\widehat{\boldsymbol{\alpha}}_k$ in (83).
**end for**
**Output** $\{\widehat{\phi}_{k,\ell}, \widehat{\alpha}_{k,\ell}\}$ and $\widehat{g}_{m,k}(\mathbf{p}_m)$.

After obtaining $\{(\widehat{\phi}_{k,\ell}, \widehat{\alpha}_{k,\ell})\}$, the effective channel under any coupler position $\mathbf{p}_m$ can be reconstructed as

$$\widehat{g}_{m,k}(\mathbf{p}_m) = \sum_{\ell=1}^{L_k} [\widehat{\boldsymbol{\alpha}}_k]_\ell \, b_m\left(\widehat{\phi}_{k,\ell}; \mathbf{p}_m\right). \tag{85}$$

The main steps of the proposed centralized channel estimation procedure are summarized in Algorithm 2. The computational complexity of Algorithm 2 is dominated by the OMP-based sparse recovery and scales as $\mathcal{O}(\sum_{k=1}^K L_k\, MV\, G)$, while constructing the dictionary incurs an additional $\mathcal{O}(MVGN)$ operations. Therefore, the overall complexity is $\mathcal{O}(\sum_{k=1}^K L_k\, MV\, G + MVGN)$. In terms of communication overhead, Algorithm 2 requires each FCA to upload its length-$\tau$ received pilot vectors $\{\mathbf{y}_m^{[v]}\}_{v=1}^V$ to the CPU over $V$ pilot blocks, resulting in a communication overhead on the order of $\mathcal{O}(MV\tau)$. The centralized channel estimation scheme provides high estimation accuracy since the CPU jointly processes the pilot-correlated observations stacked over all FCAs and all pilot blocks.

### B. Distributed Channel Estimation

The centralized channel estimation approach suffers from prohibitively high computational complexity, processing cost, and latency at the CPU, especially when the BS is equipped with an extremely large FCA array with a large number of active antennas $M$ and a vast number of coupler candidate positions. We aim to design a distributed channel estimation scheme for the FCA array that achieves accuracy close to the centralized baseline, while reducing the CPU computational burden.

*1) Processing At Local Nodes:* By applying pilot correlation to (72), we obtain

$$\widehat{g}_{m,k}^{[v]} = \frac{1}{\tau} \mathbf{y}_m^{[v]} \mathbf{S}^{\mathsf{H}} \mathbf{e}_k, \tag{86}$$

where $\mathbf{e}_k$ is the $k$-th standard basis vector. Stacking $\{\widehat{g}_{m,k}^{[v]}\}_{v=1}^V$ yields the local observation vector for user $k$ as

$$\widehat{\mathbf{y}}_{m,k} = \left[\widehat{g}_{m,k}^{[1]}, \ldots, \widehat{g}_{m,k}^{[V]}\right]^{\mathsf{T}} \in \mathbb{C}^{V\times 1}. \tag{87}$$

Similar to the centralized channel estimation step, we discretize the azimuth domain into $G \gg L_k$ grid points $\{\phi_1, \ldots, \phi_G\}$ and define the local dictionary at the $m$-th FCA as

$$\mathbf{A}_m = [\mathbf{a}_m(\phi_1), \ldots, \mathbf{a}_m(\phi_G)] \in \mathbb{C}^{V\times G}, \tag{88}$$

where $[\mathbf{a}_m(\phi)]_v = b_m(\phi; \mathbf{p}_m^{[v]})$ for $v = 1, \ldots, V$. Thus, (87) can be expressed as the sparse model

$$\widehat{\mathbf{y}}_{m,k} = \mathbf{A}_m\, \mathbf{x}_{m,k} + \mathbf{n}_{m,k}, \tag{89}$$

where $\mathbf{x}_{m,k} \in \mathbb{C}^{G\times 1}$ is sparse and its support encodes the azimuth angles of user $k$ on the grid. The support is common across $m$ since these angles are global parameters shared by all FCAs. Moreover, $\mathbf{n}_{m,k} \sim \mathcal{CN}(\mathbf{0}, \sigma_{m,\text{eff}}^2 \mathbf{I}_V)$ denotes the effective noise vector after pilot correlation and stacking over the $V$ pilot blocks, with $\sigma_{m,\text{eff}}^2 = \sigma_m^2/\tau$.

To convey support information with low overhead, the $m$-th FCA computes a matched-filter proxy $\mathbf{c}_{m,k} = \mathbf{A}_m^{\mathsf{H}} \widehat{\mathbf{y}}_{m,k}$ and its normalized energy $\rho_{m,k}(j) = \frac{|[\mathbf{c}_{m,k}]_j|^2}{\|\mathbf{a}_m(\phi_j)\|_2^2 + \epsilon_{\text{n}}}$, $j = 1, \ldots, G$, where $\epsilon_{\text{n}} > 0$ avoids numerical issues when $\|\mathbf{a}_m(\phi_j)\|_2^2$ is small. It then selects a candidate support set via noise-calibrated hard thresholding [27]:

$$\mathcal{I}_{m,k} = \left\{ j \in \{1, \ldots, G\} \;\middle|\; \rho_{m,k}(j) \geq \eta\, \sigma_{m,\text{eff}}^2 \right\}, \tag{90}$$

where $\eta > 0$ controls the pruning aggressiveness. Finally, the $m$-th FCA uploads only the index-value pairs $\mathcal{U}_{m,k} = \{(j, \rho_{m,k}(j))\}_{j\in\mathcal{I}_{m,k}}$ to the CPU. Since the azimuth domain is sparse, the uploaded list is typically low-dimensional, i.e., $|\mathcal{I}_{m,k}| \ll G$ in typical multipath channels.

*2) Processing At Central Node:* Since azimuth angles $\{\phi_{k,\ell}\}_{\ell=1}^{L_k}$ are path-level geometric parameters and thus common to all FCAs, they are global parameters shared across different FCAs. Local index set $\{\mathcal{I}_{m,k}\}$ provides complementary evidence of this common support on the grid. Accordingly, the CPU forms an aggregated grid score for each $j \in \{1, \ldots, G\}$ as

$$s_k(j) = \sum_{m=1}^M \mathbf{1}(j \in \mathcal{I}_{m,k})\, \rho_{m,k}(j), j = 1, \ldots, G, \tag{91}$$

where $\mathbf{1}(j \in \mathcal{I}_{m,k})$ equals 1 if $j \in \mathcal{I}_{m,k}$ and equals 0 otherwise, so that only the locally retained indices contribute to $s_k(j)$. Then, the CPU estimates the support by selecting the $L_k$ grid points that yield the largest aggregated score, namely,

$$\widehat{\Omega}_k = \arg \max_{\Omega\subseteq\{1,\ldots,G\}, |\Omega|=L_k} \sum_{j\in\Omega} s_k(j). \tag{92}$$

Here, $\widehat{\Omega}_k = \{\widehat{\jmath}_{k,1}, \ldots, \widehat{\jmath}_{k,L_k}\}$ denotes the selected indices after sorting in descending order such that $s_k(\widehat{\jmath}_{k,1}) \geq \cdots \geq s_k(\widehat{\jmath}_{k,L_k})$. The estimated azimuth angles are then obtained by mapping the selected grid indices to the corresponding grid

Authorized licensed use limited to: Nanjing University. Downloaded on October 30,2026 at 06:12:46 UTC from IEEE Xplore. Restrictions apply.

**Algorithm 3:** Distributed Channel Estimation for FCA Systems.

**Input** $\mathbf{S}$, $\tau$, $V$, grid $\mathcal{G}$, $\mathbf{p}_m^{[v]}$, $\eta$, $\epsilon_{\mathrm{n}}$, and $\epsilon_k$.
**Processing at local nodes**
**for** $v = 1$ to $V$ **do**
  For each FCA $m$ **in parallel**, apply $\mathbf{p}_m^{[v]}$ and receive $\mathbf{y}_m^{[v]}$.
  For each FCA $m$ **in parallel**, compute $\widehat{g}_{m,k}^{[v]}$ for all $k$ via (86).
**end for**
**for** each FCA $m$ **in parallel** and each user $k$ **do**
  Form $\widehat{\mathbf{y}}_{m,k}$ via (87) and build $\mathbf{A}_m$ via (88).
  Compute $\mathbf{c}_{m,k}$ and $\rho_{m,k}(j)$.
  Compute $\mathcal{I}_{m,k}$ via (90) and upload $\mathcal{U}_{m,k}$ to the CPU.
**end for**
**Processing at central node**
**for** each user $k$ at the CPU **do**
  Compute $s_k(j)$ via (91) and obtain $\widehat{\Omega}_k$ via (92).
  Obtain $\{\widehat{\phi}_{k,\ell}\}$ via (93) and broadcast $\widehat{\Omega}_k$.
**end for**
**Post-processing at local nodes**
**for** each FCA $m$ **in parallel** and each user $k$ **do**
  Form $\mathbf{A}_{m,k}^{\mathrm{g}}$ via (94).
  Compute $(\mathbf{R}_{m,k}, \mathbf{q}_{m,k})$ via (96) and upload them to the CPU.
**end for**
**Post-processing at central node**
**for** each user $k$ at the CPU **do**
  Aggregate $(\mathbf{R}_k, \mathbf{q}_k)$ via (97) and compute $\widehat{\boldsymbol{\alpha}}_k$ via (98).
  Broadcast $\widehat{\boldsymbol{\alpha}}_k$.
**end for**
**Output** $\{\widehat{\phi}_{k,\ell}, \widehat{\alpha}_{k,\ell}\}$ and $\widehat{g}_{m,k}(\mathbf{p}_m)$.

points as

$$\widehat{\phi}_{k,\ell} = \phi_{\widehat{\jmath}_{k,\ell}}, \ell = 1, \ldots, L_k. \tag{93}$$

*3) Post-Processing At Local Nodes:* The CPU broadcasts the estimated support set, $\widehat{\Omega}_k$, to all FCAs. Given $\widehat{\Omega}_k$, the $m$-th FCA restricts its local dictionary to the columns indexed by $\widehat{\Omega}_k$, namely,

$$\mathbf{A}_{m,k}^{\mathrm{g}} = [\mathbf{a}_m(\phi_j)]_{j\in\widehat{\Omega}_k} \in \mathbb{C}^{V\times L_k}, \tag{94}$$

where $\mathbf{a}_m(\phi_j) \in \mathbb{C}^{V\times 1}$ is the $m$-th local steering vector across the $V$ pilot blocks associated with grid angle $\phi_j$. Then, the local sparse recovery problem reduces to estimating the complex path gains on the reduced support. Specifically, local stacked observation $\widehat{\mathbf{y}}_{m,k} \in \mathbb{C}^{V\times 1}$ follows the following low-dimensional linear model,

$$\widehat{\mathbf{y}}_{m,k} = \mathbf{A}_{m,k}^{\mathrm{g}}\, \boldsymbol{\alpha}_k + \mathbf{n}_{m,k}, \tag{95}$$

where $\boldsymbol{\alpha}_k \in \mathbb{C}^{L_k\times 1}$ collects the path gains aligned with the ordering of indices in $\widehat{\Omega}_k$. The reduced model allows each FCA to contribute to estimating the path gains using only a few coefficients, instead of processing the full $G$-dimensional sparse vector.

To avoid sending the $V$-dimensional observation $\widehat{\mathbf{y}}_{m,k}$ from each FCA, the $m$-th FCA computes and forwards the following sufficient statistics for LS estimation to the CPU,

$$\mathbf{R}_{m,k} = (\mathbf{A}_{m,k}^{\mathrm{g}})^{\mathsf{H}}\mathbf{A}_{m,k}^{\mathrm{g}} \in \mathbb{C}^{L_k\times L_k}, \tag{96a}$$

$$\mathbf{q}_{m,k} = (\mathbf{A}_{m,k}^{\mathrm{g}})^{\mathsf{H}}\widehat{\mathbf{y}}_{m,k} \in \mathbb{C}^{L_k\times 1}, \tag{96b}$$

so that the CPU can recover the global LS solution by aggregating $\sum_m \mathbf{R}_{m,k}$ and $\sum_m \mathbf{q}_{m,k}$, while the uplink overhead scales with $L_k$ rather than $V$.

*4) Post-Processing At Central Node:* After receiving LS sufficient statistics $\{\mathbf{R}_{m,k}, \mathbf{q}_{m,k}\}_{m=1}^M$ from all FCAs, the CPU aggregates them as

$$\mathbf{R}_k = \sum_{m=1}^M \mathbf{R}_{m,k}, \quad \mathbf{q}_k = \sum_{m=1}^M \mathbf{q}_{m,k}. \tag{97}$$

Estimating the path gain vector, $\boldsymbol{\alpha}_k \in \mathbb{C}^{L_k\times 1}$, on fixed support $\widehat{\Omega}_k$ amounts to solving normal equation $\mathbf{R}_k\boldsymbol{\alpha}_k = \mathbf{q}_k$. To improve numerical stability when $\mathbf{R}_k$ is ill-conditioned, we apply diagonal loading and estimate the path-gain vector as

$$\widehat{\boldsymbol{\alpha}}_k = (\mathbf{R}_k + \epsilon_k \mathbf{I}_{L_k})^{-1}\, \mathbf{q}_k \in \mathbb{C}^{L_k\times 1}, \tag{98}$$

where $\epsilon_k > 0$ is a small constant. Note that (98) only requires each antenna to transmit the sufficient statistics $(\mathbf{R}_{m,k}, \mathbf{q}_{m,k})$, whose dimension scales with $L_k$ rather than the pilot block length $V$.

After obtaining $\{\widehat{\Omega}_k, \widehat{\boldsymbol{\alpha}}_k\}_{k=1}^K$ from the CPU, the $m$-th FCA reconstructs its effective scalar channel under any coupler position $\mathbf{p}_m$ as in (85). The reconstructed CSI is utilized for the subsequent coupler position optimization and digital precoding procedures described in Section III.

The main steps of the proposed distributed channel estimation procedure are summarized in Algorithm 3. The computational complexity is dominated by pilot correlation and local proxy evaluation, and it scales as $\mathcal{O}(MV\tau K + KMVG + KL_k^3)$. Compared with the centralized channel estimation algorithm, the distributed channel estimation implementation substantially reduces the CPU-side computational burden and processing latency, especially when array size $M$ and candidate grid size $G$ are large. In terms of communication overhead, the distributed channel estimation scheme exchanges only low-dimensional LS sufficient statistics $\{\mathbf{R}_{m,k}, \mathbf{q}_{m,k}\}$ for each user $k$, whose communication load scales as $\mathcal{O}(MKL_k^2)$.

## V. Simulation Results

In this section, numerical results are presented to evaluate the performance of the proposed distributed FCA system design. The coupler movement region associated with each active antenna is modeled as a square with side length $A$. In the simulations, both the active antennas and the passive couplers are modeled as identical thin straight-wire dipoles of length $D = \lambda/2$, aligned with the $z$-axis. The self-impedance entries corresponding to $i = j$ in (16) are computed using the closed-form expressions given in (8-60a) and (8-60b) of [28]. The active antennas are placed with an inter element spacing of $d_y = 2.2\,\lambda$. Each coupler is allowed to move within a square region of side length $A = 2\,\lambda$, subject to a minimum element spacing constraint of $d_{\min} = 0.15\,\lambda$. The carrier frequency is set to $f_c = 7$ GHz. The load-impedance matrix $\mathbf{X}$ is diagonal with identical entries $0.05 + j50\,\Omega$.

Authorized licensed use limited to: Nanjing University. Downloaded on October 30,2026 at 06:12:46 UTC from IEEE Xplore. Restrictions apply.

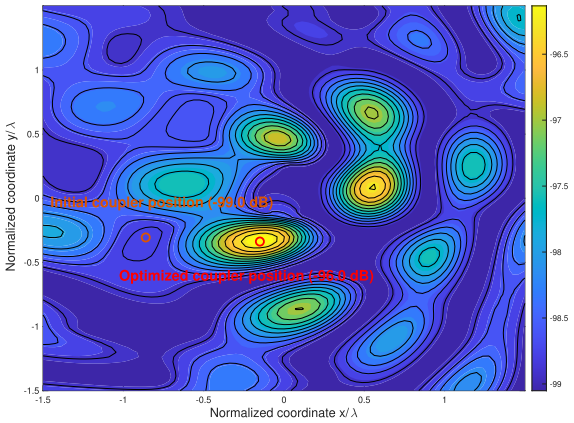



Fig. 3. Channel power gain (dB) between the FCA array and the user with $N = 1$, $K = 1$, $M = 5$, $P = 30$ dBm, and $L_k = 15$.

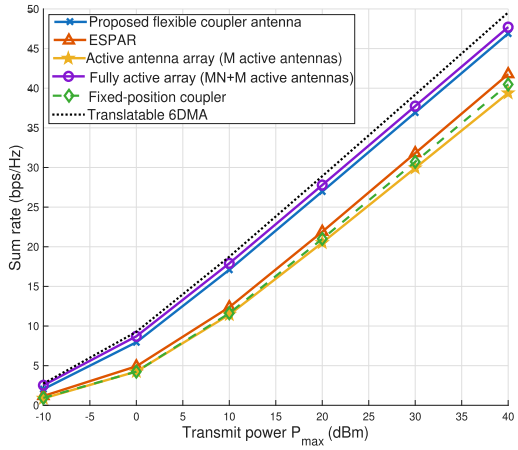



Fig. 4. Achievable rate versus maximum transmit power for different schemes with $N = 2$, $K = 3$, $M = 15$, and $L_k = 15$.

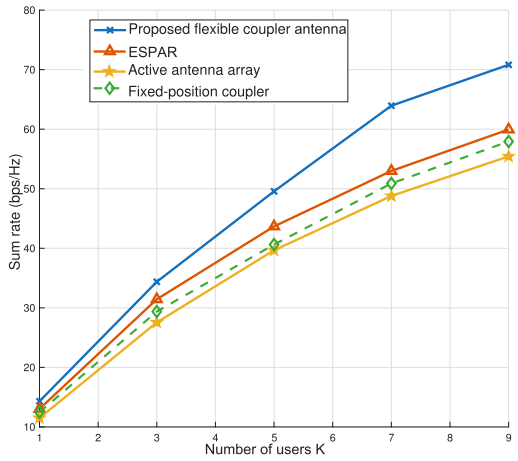



Fig. 5. Achievable rate versus number of users with $N = 2$, $M = 10$, $P = 30$ dBm, and $L_k = 15$.

### A. *Performance of Coupler Position Optimization*

To evaluate the performance of coupler position optimization, the proposed FCA scheme is compared with the following baseline schemes.

- *Active antenna array:* The transmitter has $M$ active antennas without any coupler elements.
- *Fixed-position coupler:* The $N$ couplers are fixed at uniformly spaced positions around the active antenna with spacing $0.4\,\lambda$, and the load impedance matrix $\mathbf{X}$ has constant diagonal entries of $0.05 + j50\,\Omega$.
- *Electronically steerable parasitic array radiator (ESPAR) [29]:* Closed-form optimization of load impedance matrix $\mathbf{X}$ is used to maximize the sum rate while keeping the coupler positions fixed at the same positions as in the fixed-position coupler case.
- *Fully active array:* All $MN + M$ ports are configured as active antennas and uniformly placed at fixed positions within each movement region.
- *Translatable 6DMA:* All $N + 1$ ports are active antennas, each allowed to translate within a region of the same size as the coupler movement region [30], [31].

To demonstrate the effect of coupler position optimization on channel characteristics, Fig. 3 shows a representative realization of the channel power gain in dB as a function of the coupler position within its feasible movement region. As can be seen, the channel power gain presents a highly irregular spatial distribution with multiple local extrema, which implies that even sub-wavelength coupler movements can significantly modify the mutual-impedance-induced currents and, consequently, the effective channel under rich multipath propagation. In particular, starting from an initial coupler location with a gain of $-99.0$ dB, the proposed algorithm steers the coupler toward a more favorable local optimum highlighted in the figure, thereby increasing the gain to $-96.0$ dB.

Fig. 4 plots the achievable sum rate versus maximum transmit power $P_{\max}$ for the proposed FCA array and several baseline schemes. As $P_{\max}$ increases, all schemes achieve higher rates due to the improved effective signal-to-noise ratio (SNR). It is observed that the proposed FCA array closely approaches the fully active array with $MN + M$ RF chains while using only $M$ active antennas. This gain is achieved because coupler position optimization provides substantial mechanical beamforming and fading mitigation gains in rich multipath channels while maintaining a limited RF chain cost. In contrast, the ESPAR optimizes only the load impedances with fixed coupler locations and therefore cannot fully exploit the spatial degree of freedom (DoF) offered by position reconfiguration [29], [32]. Moreover, the fixed position coupler and the active antenna array exhibit lower rates due to their fixed geometries and the lack of a reconfigurable aperture. Although the translatable 6DMA achieves the highest rate among all schemes, the proposed FCA remains close to its performance while requiring fewer RF chains [33].

In Fig. 5, we plot the achievable sum rate versus the number of users $K$ for the proposed FCA array and benchmark schemes. As $K$ increases, the sum rate improves for all schemes due to the increased spatial multiplexing gain, while the growth gradually slows down since stronger multiuser interference must be mitigated under a fixed transmit power budget. Compared with the ESPAR and fixed position coupler schemes, the proposed design consistently achieves a higher sum rate. This performance advantage becomes more pronounced at moderate and large values of $K$, where MMSE based multiuser precoding is more

Authorized licensed use limited to: Nanjing University. Downloaded on October 30,2026 at 06:12:46 UTC from IEEE Xplore. Restrictions apply.

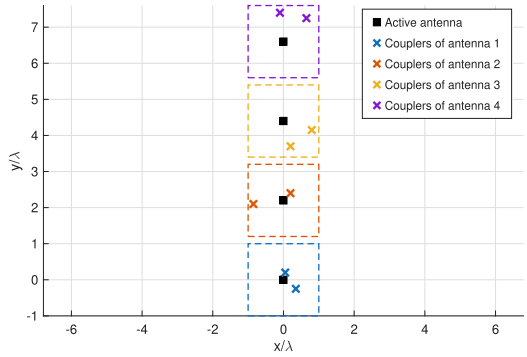



Fig. 6. Optimized coupler positions obtained by the proposed algorithm with $K = 2$, $M = 4$, $L_k = 15$, and $N = 2$.

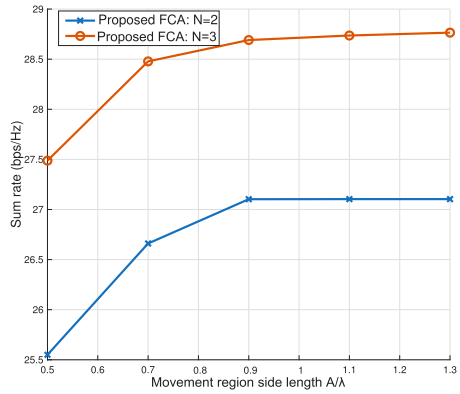



Fig. 7. Achievable rate versus movement region size with $K = 3$, $M = 4$, and $L_k = 15$.

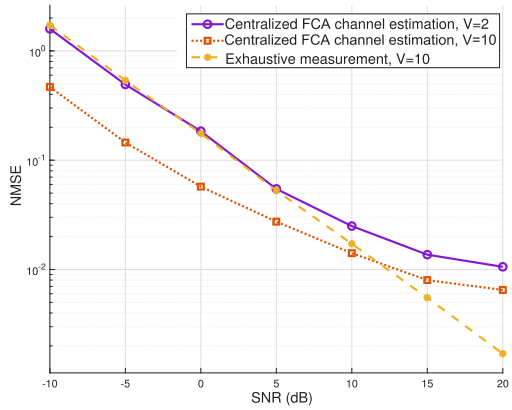



Fig. 8. NMSE versus SNR for different $V$ with $K = 2$, $M = 8$, $N = 2$, $\tau = 13$, and $L_k = 3$.

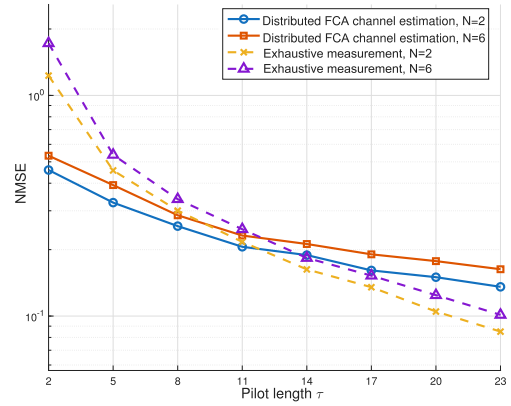



Fig. 9. NMSE versus pilot length for different $N$ with $K = 2$, $M = 4$, SNR $= 0$ dB, and $L_k = 3$.

sensitive to the conditioning of the effective channel matrix and thus benefits more from geometry reconfiguration, whereas the benchmark schemes with fixed geometries cannot adapt to user induced interference coupling.

Fig. 6 shows the numerically optimized coupler positions around each fixed active antenna. It can be observed that, due to rich multipath propagation and multiuser transmission, the optimal coupler constellations differ across active antennas. Specifically, the superposition of dominant propagation paths varies from one antenna to another, and the desired signal and inter user interference contributions are location dependent because of the coupled electromagnetic response. As a result, the optimized coupler geometries and mechanical beamforming weights jointly enhance the effective channels of the intended users while suppressing multiuser interference through position-dependent mutual impedance.

In Fig. 7, the achievable sum rate is illustrated as a function of the normalized movement-region side length $A/\lambda$. It can be seen that enlarging $A/\lambda$ enhances the achievable rate for both configurations, while the improvement gradually saturates as $A/\lambda$ increases. This behavior suggests that near-optimal performance can be attained with a finite movement region. For small values of $A/\lambda$, the allowable coupler positions are severely restricted, which constrains the effective aperture and reduces the diversity of the position-dependent mutual impedance, thereby weakening the resulting mechanical beamforming gain. As $A/\lambda$ increases, position optimization becomes more effective in shaping the induced currents and mitigating unfavorable channel conditions, leading to improved sum rate. Moreover, the case with $N = 3$ consistently achieves a higher sum rate than $N = 2$ due to the additional passive elements and the resulting stronger reconfigurability.

### B. Channel Estimation Performance

Next, simulations are conducted to validate the effectiveness of the proposed distributed and centralized FCA channel estimation algorithms. The normalized mean square error (NMSE) results are obtained by averaging over all users and 500 Monte Carlo trials.

In Fig. 8, we plot the NMSE versus the average received SNR for the proposed centralized FCA channel estimation with different numbers of pilot blocks $V$. We adopt exhaustive measurement as a high-overhead benchmark scheme, where the coupler movement region is discretized into a large number ($E = 400$) of candidate locations and the effective channel is sequentially measured over all candidates, resulting in on the order of $MND$ measurements per pilot block. From Fig. 8, it can be seen that increasing $V$ significantly improves the NMSE performance of all schemes, especially in the low to medium SNR regime, since varying the coupler positions across

Authorized licensed use limited to: Nanjing University. Downloaded on October 30,2026 at 06:12:46 UTC from IEEE Xplore. Restrictions apply.

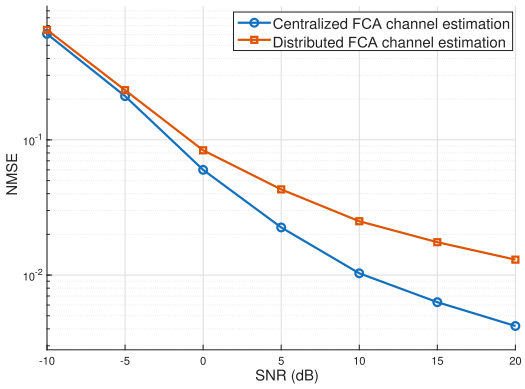



Fig. 10. NMSE comparison between the centralized and distributed channel estimation schemes with $K = 2$, $M = 4$, $N = 2$, $V = 4$, $\tau = 32$, and $L_k = 10$.

blocks generates more diversified effective channel observations and enhances angular sparse reconstruction through stacked measurements. Moreover, as observed from Fig. 8, exhaustive measurement becomes more competitive at high SNR due to its dense direct sampling with high computational complexity. In contrast, the proposed FCA method with a larger $V$ achieves lower NMSE at low SNR, since joint sparse reconstruction across blocks provides an inherent noise-averaging effect while requiring substantially fewer measurements.

In Fig. 9, we plot the NMSE versus the pilot length $\tau$ for the proposed distributed FCA channel estimation and exhaustive measurement, under two coupler numbers $N \in \{2, 6\}$. It is observed that increasing $\tau$ improves the estimation accuracy for all schemes, since longer pilot sequences enhance the reliability of the pilot correlation outputs. In the short pilot regime, the proposed distributed method achieves lower NMSE than exhaustive measurement for both values of $N$, as it exploits structured sparsity and performs fusion using low-dimensional sufficient statistics, which provides effective noise suppression when pilots are limited. As $\tau$ increases, exhaustive measurement becomes more competitive due to its dense direct sampling. Moreover, increasing $N$ leads to higher NMSE for both schemes, indicating a higher pilot requirement to maintain the same estimation accuracy.

In Fig. 10, we compare the NMSE performance of the proposed centralized and distributed FCA channel estimation schemes versus the average receive SNR. Both schemes achieve lower NMSE as the SNR increases. Moreover, the centralized scheme consistently outperforms the distributed one over the entire SNR range, as it can jointly exploit the sparsity structure across all antennas and users, whereas the distributed scheme relies on local processing at FCAs with limited information fusion. Nevertheless, the distributed scheme provides a favorable accuracy-complexity tradeoff by shifting computations to the LPUs and exchanging only low-dimensional sufficient statistics.

## VI. Conclusion

We have proposed a distributed FCA array that enables mechanical beamforming through passive coupler repositioning around fixed active antennas, supported by a distributed architecture with local LPUs and a CPU. We have also investigated pilot-assisted centralized and distributed channel estimation solutions for the FCA array. Simulation results validate the performance of the proposed FCA array and channel estimation algorithms compared with benchmark schemes. In the proposed FCA array, reconfigurable passive coupler positioning provides a cost-effective way to enhance communication performance without the need to add more RF chains. Moreover, the compact form factor and small footprint of the FCA array make it particularly appealing for devices with stringent size, weight, and power (SWAP) constraints. For the future work, we will apply the proposed FCA array to support diverse applications and services, such as being mounted on unmanned aerial vehicles (UAVs) with limited payload in the low-altitude economy. Beyond communications, we will investigate FCA-enabled target sensing to achieve a more favorable sensing-communication tradeoff in integrated sensing and communication (ISAC) systems.

## References

[1] C. You et al., "Next generation advanced transceiver technologies for 6G and beyond," *IEEE J. Sel. Areas Commun.*, vol. 43, no. 3, pp. 582–627, Mar. 2025.

[2] Z. Chen, E. Bjornson, and E. G. Larsson, "Dynamic resource allocation in co-located and cell-free massive MIMO," *IEEE Trans. Green Commun. Netw.*, vol. 4, no. 1, pp. 209–220, Mar. 2020.

[3] M. Kumar et al., "Distributed machine learning approach for low-latency localization in cell-free massive MIMO systems," 2025, *arXiv:2507.14216*.

[4] C.-X. Wang et al., "On the road to 6G: Visions, requirements, key technologies, and testbeds," *IEEE Commun. Surv. Tut.*, vol. 25, no. 2, pp. 905–974, Secondquarter 2023.

[5] Z. Wang et al., "A tutorial on extremely large-scale MIMO for 6G: Fundamentals, signal processing, and applications," *IEEE Commun. Surv. Tut.*, vol. 26, no. 3, pp. 1560–1605, thirdquarter 2024.

[6] M. Di Renzo et al., "Smart radio environments empowered by reconfigurable intelligent surfaces: How it works, state of research, and the road ahead," *IEEE J. Sel. Areas Commun.*, vol. 38, no. 11, pp. 2450–2525, Nov. 2020.

[7] X. Yu, D. Xu, Y. Sun, D. W. K. Ng, and R. Schober, "Robust and secure wireless communications via intelligent reflecting surfaces," *IEEE J. Sel. Areas Commun.*, vol. 38, no. 11, pp. 2637–2652, Nov. 2020.

[8] X. Shao, C. You, W. Ma, X. Chen, and R. Zhang, "Target sensing with intelligent reflecting surface: Architecture and performance," *IEEE J. Sel. Areas Commun.*, vol. 40, no. 7, pp. 2070–2084, Jul. 2022.

[9] Q. Wu et al., "Intelligent surfaces empowered wireless network: Recent advances and the road to 6G," *Proc. IEEE*, vol. 112, no. 7, pp. 724–763, Jul. 2024.

[10] R. Li, S. Sun, and M. Tao, "Atomic norm minimization-based DoA estimation for IRS-assisted sensing systems," *IEEE Wireless Commun. Lett.*, vol. 13, no. 10, pp. 2672–2676, Oct. 2024.

[11] Y. Xu, E. G. Larsson, E. A. Jorswieck, X. Li, S. Jin, and T.-H. Chang, "Distributed signal processing for extremely large-scale antenna array systems: State-of-the-art and future directions," *IEEE J. Sel. Topics Signal Process.*, vol. 19, no. 2, pp. 304–330, Mar. 2025.

[12] G. Zhu, Y. Wang, and K. Huang, "Broadband analog aggregation for low-latency federated edge learning," *IEEE Trans. Wireless Commun.*, vol. 19, no. 1, pp. 491–506, Jan. 2020.

[13] B. Sirkeci-Mergen and A. Scaglione, "Randomized space-time coding for distributed cooperative communication," *IEEE Trans. Signal Process.*, vol. 55, no. 10, pp. 5003–5017, Oct. 2007.

[14] T. Charalambous, M. G. Rabbat, M. Johansson, and C. N. Hadjicostis, "Distributed finite-time computation of digraph parameters: Left-eigenvector, out-degree and spectrum," *IEEE Trans. Control Netw. Syst.*, vol. 3, no. 2, pp. 137–148, Jun. 2016.

[15] X. Shao, Q. Jiang, and R. Zhang, "6D movable antenna based on user distribution: Modeling and optimization," *IEEE Trans. Wireless Commun.*, vol. 24, no. 1, pp. 355–370, Jan. 2025.

Authorized licensed use limited to: Nanjing University. Downloaded on October 30,2026 at 06:12:46 UTC from IEEE Xplore. Restrictions apply.

[16] X. Shao, R. Zhang, Q. Jiang, and R. Schober, "6D movable antenna enhanced wireless network via discrete position and rotation optimization," *IEEE J. Sel. Areas Commun.*, vol. 43, no. 3, pp. 674–687, Mar. 2025.
[17] X. Shao and R. Zhang, "6DMA enhanced wireless network with flexible antenna position and rotation: Opportunities and challenges," *IEEE Commun. Mag.*, vol. 63, no. 4, pp. 121–128, Apr. 2025.
[18] Y. Li et al., "AI signal processing paradigm for movable antenna: From spatial position optimization to electromagnetic reconfigurability," 2025, *arXiv:2510.19209*.
[19] N. Cheng et al., "Channel knowledge map-enabled 6D movable antenna systems with kinematic constraints: A manifold optimization approach," *IEEE Trans. Wireless Commun.*, vol. 25, pp. 8968–8981, 2026.
[20] X. Shao, R. Zhang, Q. Jiang, J. Park, T. Q. S. Quek, and R. Schober, "Distributed channel estimation and optimization for 6D movable antenna: Unveiling directional sparsity," *IEEE J. Sel. Topics Signal Process.*, vol. 19, no. 2, pp. 349–365, Mar. 2025.
[21] A. Kalis, A. G. Kanatas, and C. B. Papadias, *Parasitic Antenna Arrays for Wireless MIMO Systems*. New York, NY, USA: Springer, 2014.
[22] V. Lara and K. Dechoum, "Kirchhoff's voltage law corrected for radiating circuits," *Revista Brasileira de Ensino de Fısica*, vol. 37, no. 1, 2015, Art. no. 1307.
[23] M. T. Ivrlač and J. A. Nossek, "Toward a circuit theory of communication," *IEEE Trans. Circuits Syst. I., Reg. Papers*, vol. 57, no. 7, pp. 1663–1683, Jul. 2010.
[24] D. H. Nguyen and T. Le-Ngoc, "MMSE precoding for multiuser MISO downlink transmission with non-homogeneous user SNR conditions," *EURASIP J. Adv. Signal Process.*, vol. 2014, no. 1, 2014, Art. no. 85.
[25] A. Nedic and A. Ozdaglar, "Distributed subgradient methods for multi-agent optimization," *IEEE Trans. Autom. Control*, vol. 54, no. 1, pp. 48–61, Jan. 2009.
[26] G. Tan and T. Herfet, "A framework of analyzing OMP-based channel estimations in mobile OFDM systems," *IEEE Wireless Commun. Lett.*, vol. 5, no. 4, pp. 408–411, Aug. 2016.
[27] M. F. Duarte, S. Sarvotham, D. Baron, M. B. Wakin, and R. G. Baraniuk, "Distributed compressed sensing of jointly sparse signals," in *Proc. Asilomar Conf. Signals, Sys., Comput*, 2005, pp. 1537–1541.
[28] C. A. Balanis, *Antenna Theory: Analysis and Design*. Hoboken, NJ, USA: Wiley, 2016.
[29] H. Kawakami and T. Ohira, "Electrically steerable passive array radiator (ESPAR) antennas," *IEEE Antennas Propag. Mag.*, vol. 47, no. 2, pp. 43–50, Apr. 2005.
[30] X. Shao et al., "A tutorial on six-dimensional movable antenna for 6G networks: Synergizing positionable and rotatable antennas," *IEEE Commun. Surv. Tut.*, vol. 28, pp. 3666–3709, 2026.
[31] X. Shao et al., "Polarforming antenna enhanced sensing and communication: Modeling and optimization," *IEEE J. Sel. Areas Commun.*, vol. 44, pp. 416–431, 2026.
[32] A. Mezghani et al., "Reincorporating circuit theory into information theory," *IEEE BITS Inf. Theory Mag.*, vol. 4, no. 1, pp. 40–58, Mar. 2024.
[33] X. Shao et al., "Hybrid near-far field 6D movable antenna design exploiting directional sparsity and deep learning," *IEEE Trans. Wireless Commun.*, vol. 25, pp. 3736–3749, 2026.



**Xiaodan Shao** (Member, IEEE) received the Ph.D. degree in information and communication engineering from Zhejiang University, Hangzhou, China. She was a Humboldt Research Fellow with the Institute for Digital Communications, Friedrich-Alexander-University Erlangen-Nuremberg (FAU), Erlangen, Germany. She is currently a Postdoctoral Fellow with the Department of Electrical and Computer Engineering, University of Waterloo, Waterloo, ON, Canada. Her research interests include six-dimensional movable antenna (6DMA), flexible coupler antenna (FCA), MIMO, statistical signal processing, and machine learning for wireless communication. She was the recipient of the IEEE Communications Society Leonard G. Abraham Prize in 2025, IEEE GLOBECOM Best Paper Award in 2025, IEEE VTC Best Paper Award in 2025, IEEE WCSP Best Paper Award in 2020, and Best Ph.D. Thesis Award of China Institute of Communications in 2023. She serves as an Associate Editor for IEEE WIRELESS COMMUNICATIONS LETTERS and IEEE TRANSACTIONS ON COMMUNICATIONS.



**Chuangye Shan** is currently a Senior Development Engineer with Shell (Beijing) New Energy Technology Company, Ltd., Beijing, China. He was a Technical Manager with Shanghai Mingsheng Quality Artificial Intelligence Technology Company, Ltd. His research interests include artificial intelligence, flexible antennas, and optimization methods. He was the recipient of the First Prize in the Blue Bridge Cup National Software and Information Technology Professionals Competition.



**Weihua Zhuang** (Fellow, IEEE) received the B.Sc. and M.Sc. degrees in electrical engineering from Dalian Maritime University, Dalian, China, and the Ph.D. degree in electrical engineering from the University of New Brunswick, Fredericton, NB, Canada. Since 1993, she has been a Faculty Member of the Department of Electrical and Computer Engineering, University of Waterloo, Waterloo, ON, Canada, where she is currently a University Professor and a University Research Chair in wireless communication networks. Her research interests include network architecture, algorithms and protocols, and service provisioning in future communication systems. She was the recipient of the Women's Distinguished Career Award in 2021 from the IEEE Vehicular Technology Society, R.A. Fessenden Award in 2021 from IEEE Canada, Award of Merit in 2021 from the Federation of Chinese Canadian Professionals (Ontario), and Technical Recognition Award in Ad Hoc and Sensor Networks in 2017 from the IEEE Communications Society. She is a fellow of the Royal Society of Canada (RSC), the Canadian Academy of Engineering (CAE), and the Engineering Institute of Canada (EIC). She is an Elected Member of the Board of Governors (BoG) of the IEEE Vehicular Technology Society (VTS). She was the VTS President (2023-2024) and Editor-in-Chief of IEEE TRANSACTIONS ON VEHICULAR TECHNOLOGY (2007-2013), the Editor of IEEE TRANSACTIONS ON WIRELESS COMMUNICATIONS (2005-2009), and an IEEE Communications Society Distinguished Lecturer (2008-2011).



**Xuemin (Sherman) Shen** (Fellow, IEEE) received the Ph.D. degree in electrical engineering from Rutgers University, New Brunswick, NJ, USA, in 1990. He is currently a University Professor with the Department of Electrical and Computer Engineering, University of Waterloo, Waterloo, ON, Canada. His research interests include network resource management, wireless network security, Internet of Things, 5G and beyond, and vehicular networks. He is a registered Professional Engineer of Ontario, Canada, Engineering Institute of Canada Fellow, Canadian Academy of Engineering Fellow, Royal Society of Canada Fellow, Chinese Academy of Engineering Foreign Member, and International Fellow of the Engineering Academy of Japan. He is the Past President of the IEEE ComSoc, Vice President for Technical & Educational Activities, Vice President for Publications, Member-at-Large on the Board of Governors. He was the recipient of the "West Lake Friendship Award" from Zhejiang Province in 2023, President's Excellence in Research from the University of Waterloo in 2022, Canadian Award for Telecommunications Research from the Canadian Society of Information Theory (CSIT) in 2021, R.A. Fessenden Award in 2019 from IEEE, Canada, Award of Merit from the Federation of Chinese Canadian Professionals (Ontario) in 2019, James Evans Avant Garde Award in 2018 from the IEEE Vehicular Technology Society, Joseph LoCicero Award in 2015 and Education Award in 2017 from the IEEE Communications Society (ComSoc), and Technical Recognition Award from Wireless Communications Technical Committee (2019) and AHSN Technical Committee (2013). He has also recipient of the Excellent Graduate Supervision Award in 2006 from the University of Waterloo and Premier's Research Excellence Award (PREA) in 2003 from the Province of Ontario, Canada. He serves/served as the General Chair of 6G Global Conference'23, and ACM Mobihoc'15, Technical Program Committee Chair/Co-Chair of IEEE Globecom'24, 16 and 07, IEEE Infocom'14, IEEE VTC'10 Fall, and Chair of IEEE ComSoc Technical Committee on Wireless Communications. He served as the Editor-in-Chief of IEEE IOT JOURNAL, IEEE NETWORK, and *IET Communications*.

Authorized licensed use limited to: Nanjing University. Downloaded on October 30,2026 at 06:12:46 UTC from IEEE Xplore. Restrictions apply.